NOAA Technical Report NESS 80

Calculation of Atmospheric Radiances and Brightness Temperatures in Infrared Window Channels of Satellite Radiometers

Washington, D.C.
March 1980

U.S. DEPARTMENT OF COMMERCE
National Oceanic and Atmospheric Administration
National Environmental Satellite Service

NOAA TECHNICAL REPORTS

National Environmental Satellite Service Series

ironmental Satellite Service (NESS) is respons''.e for the establishment and operation al satellite systems of NOAA.

report in NOAA Techn'c l Report NESS series will not preclude later publication in an ed form in scientific journals. NESS series of NOAA Technical Reports is a continuatains the consecutive numbering seq"anc of, the former series, ESSA Technical Report ntal Satellite Center (NESC), and of the earlier series, Weather Bureau Meteorological ry (MSL) Report. Reports 1 through 39 are listed in publication NESC 56 of this ser-

Reports in the series are available from the National Technical Information Service (NTIS), U.S. Department of Commerce, Sills Bldg., 5285 Port Royal Road, Springfield, VA 22161, in paper copy or microfiche form. Order by accession number, when given, in parentheses. Beginning with 64, printed copies of the reports, if available, can be ordered through the Superintendent of Documents, U.S. Government Printing Office, Washington, DC 20402. Prices given on request from the Superintendent of Documents or NTIS.

ESSA Technical Reports

NESC 46 Monthly and Seasonal Mean Global Charts of Brightness From ESSA 3 and ESSA 5 Digitized Pictures, February 1967-February 1 3. V. Ray Taylor and Jay S. Winston, November 1968, 9 pp. plus 17 charts. (PB-180-717)

NESC 47 A Polynomial Representation of Carbon Dioxide and Water Vapor Transmission. William L. Smith, February 1969 (reprinted April 1971), 20 pp. (PB-183-296)

NESC 48 Statistical Estimation of the Atmosphere's Geopotential Height Distribution From Satellite Radiation Measurements. William L. Smith, February 1969, 29 pp. (PB-183-297)

NESC 49 Synoptic/Dynamic Diagnosis of a Developing Low-Level Cyclone and Its Satellite-Viewed Cloud Patterns. Harold J. Brodrick and E. Paul McClain, May 1969, 26 pp. (PB-184-612)

NESC 50 Estimating Maximum Wind Speed of Tropical Storms From High Resolution Infrared Data. L. F. Hubert, A. Timchalk, and S. Fritz, May 1969, 33 pp. (PB-184-611)

NESC 51 Application of Meteorological Satellite Data in Analysis and Forecasting. Ralph K. Anderson, Jerome P. Ashman, Fred Bittner, Golden R. Farr, Edward W. Ferguson, Vincent J. Oliver, Arthur H. Smith, James F. W. Purdom, and Rance W. Skidmore, March 1974 (reprint and revision of NESC 51, September 1969, and inclusion of Supplement, November 1971, and Supplement 2, March 1973), pp. 1--6C-18 plus references.

NESC 52 Data Reduction Processes for Spinning Flat-Plate Satellite-Borne Radiometers. Torrence H. MacDonald, July 1970, 37 pp. (COM-71-00132)

NESC 53 Archiving and Climatological Applications of Meteorological Satellite Data. John A. Leese, Arthur L. Booth, and Frederick A. Godshall, July 1970, pp. 1-1--5-8 plus references and appendixes A through D. (COM-71-00076)

NESC 54 Estimating Cloud Amount and Height From Satellite Infrared Radiation Data. P. Krishna Rao, July 1970, 11 pp. (PB-194-685)

NESC 56 Time-Longitude Sections of Tropical Cloudiness (December 1966-November 1967). J. M. Wallace, July 1970, 37 pp. (COM-71-00131)

NESS 55 The Use of Satellite-Observed Cloud Patterns in Northern Hemisphere 500-mb Numerical Analysis. Roland E. Nagle and Christopher M. Hayden, April 1971, 25 pp. plus appendixes A, B, and C. (COM-73-50262)

NESS 57 Table of Scattering Function of Infrared Radiation for Water Clouds. Giichi Yamamoto, Masayuki Tanaka, and Shoji Asano, April 1971, 8 pp. plus tables. (COM-71-50312)

NESS 58 The Airborne ITPR Brassboard Experiment. W. L. Smith, D. T. Hilleary, E. C. Baldwin, W. Jacob, H. Jacobowitz, G. Nelson, S. Soules, and D. Q. Wark, March 1972, 74 pp. (COM-72-10557)

(Continued on inside back cover)

NOAA Technical Report NESS 80

Calculation of Atmospheric Radiances and Brightness Temperatures in Infrared Window Channels of Satellite Radiometers

Michael P. Weinreb and Michael L. Hill

Washington, D.C.
March 1980

U.S. DEPARTMENT OF COMMERCE
Philip M. Klutznick, Secretary

National Oceanic and Atmospheric Administration
Richard A. Frank., Administrator

National Environmental Satellite Service
David S. Johnson, Director

National Oceanic and Atmospheric Administration
TIROS Satellites and Satellite Meteorology

ERRATA NOTICE

One or more conditions of the original document may affect the quality of the image, such as:

Discolored pages
Faded or light ink
Binding intrudes into the text

This has been a co-operative project between the NOAA Central Library and the Climate Database Modernization Program, National Climate Data Center (NCDC). To view the original document contact the NOAA Central Library in Silver Spring, MD at (301) 713-2607 x124 or Library.Reference@noaa.gov.

HOV Services
Imaging Contractor
12200 Kiln Court
Beltsville, MD 20704-1387
January 26, 2009

CONTENTS

TABLES

FIGURES

CALCULATION OF ATMOSPHERIC RADIANCES AND BRIGHTNESS TEMPERATURES IN INFRARED WINDOW CHANNELS OF SATELLITE RADIOMETERS

Michael P. Weinreb and Michael L. Hill
Office of Research, National Environmental Satellite Service,
NOAA, Washington, D.C. 20233

ABSTRACT. We describe a method of simulating measurements of atmospheric radiances and brightness temperatures in wide-band window channels (at 11 and 3.7 μm) of satellite radiometers. As input the simulation takes vertical profiles of atmospheric temperature and water-vapor mixing ratio, as well as the spectral response functions of the window channels. It models the atmospheric transmittances and integrates the equation of radiative transfer. We demonstrate the use of the method with applications to the Advanced Very High Resolution Radiometer on the TIROS-N satellite.

1. INTRODUCTION

The environmental satellites operated by NOAA's National Environmental Satellite Service (NESS) carry instruments that measure the intensity of radiation upwelling from the earth's surface in the infrared "windows" at wavelengths near 11 μm and 3.7 μm. Among these instruments are the Scanning Radiometers (SR) on the ITOS 1 and NOAA 2-5 satellites, the Very High Resolution Radiometers (VHRR) on the NOAA 2-5 satellites, the Visible and Infrared Spin-Scan Radiometers (VISSR) on the current SMS/GOES satellites, and the Advanced VHRR's (AVHRR) on the current TIROS-N series of satellites. Windows are spectral intervals in which the atmosphere is nearly transparent to the radiation emitted by the earth's surface. Although the atmosphere's effect on the radiation is small, it is, nevertheless, not negligible. For example, in the 11-μm region a moist atmosphere may attenuate the radiation emitted by the earth's surface to space by 5-10%. Therefore, to infer properties of the surface from measurements in windows, we need to model theoretically the radiative transfer in the atmosphere.

This report documents a procedure for computing, in the 11- and 3.7-μm windows, the radiances and brightness temperatures that would be measured by an orbiting radiometer, given the temperature of the earth's surface and the vertical temperature and water-vapor profiles of the atmosphere. The model also takes into account other gases that absorb and emit radiation at these wavelengths. For the instruments considered here, which view in the nadir or near-nadir, these gases are carbon dioxide, nitrogen, nitrous oxide, and methane. The computations apply to spectral intervals whose widths range from several tens to several hundreds of cm^{-1}. A computer program that incorporates the method described in this paper is currently in use at NESS. Copies of this program are available on request.

The literature describes a number of earlier transmittance models that have been applied in the 11-μm window (Wark et al. 1962, Davis and Viezee 1964, Saiedy and Hilleary 1967, Anding and Kauth 1969, Smith et al. 1970, and Maul and Sidran 1973). These works were published before the importance of the self-broadened water-vapor continuum (Bignell 1970) was recognized. More recently the computer code LOWTRAN (McClatchey et al. 1972, Selby et al. 1978) was developed for modelling radiative transfer in the atmosphere in 20-cm^{-1} intervals throughout the infrared spectrum, including both the 11-μm and 3.7-μm window regions.

The method described in this report evolved from the algorithm (Wark et al. 1974, Weinreb and Neuendorffer 1973) developed at NESS to calculate radiances in the 11-μm window channel of the Vertical Temperature Profile Radiometers (VTPR) (McMillin et al. 1973) on the NOAA 2-5 satellites.

The present method has the following new features:

1. It can be applied to spectral intervals that are several hundred cm^{-1} in width. (The VTPR interval was about 8 cm^{-1} in width.)

2. It applies in both the 3.7- and the 11-μm windows.

3. It incorporates recent advances in calculating transmittances, particularly those in modelling the nitrogen absorption near 4 μm and the water-vapor continua in the 11- and 3.7-μm regions.

Section 2 of this report introduces the radiative transfer equation and describes our techniques of calculating radiances and brightness temperatures while coping with the variation of the Planck function over the considerable width (in wavenumber) of the spectral intervals. Section 3 describes the transmittance calculations, which include the effects of H_2O lines and continua, the collision-induced N_2 band near 4 μm, and the "uniformly mixed" gases, particularly CO_2, CH_4, and N_2O. Section 4 describes the numerical procedures for calculating transmittances and integrating the radiative transfer equation. The report concludes with a few applications of the calculations to the AVHRR on TIROS-N.

2. APPLICATION OF THE RADIATIVE TRANSFER EQUATION IN WIDE SPECTRAL INTERVALS

2.1 The Radiative Transfer Equation

The upwelling radiance $R(\nu)$ at wavenumber ν can be calculated from knowledge of the temperature of the earth's surface, the atmospheric vertical temperature profile, and the vertical profiles of concentrations of the gases that absorb radiation at ν. We accomplish this by numerically integrating the equation of radiative transfer in its integral form (see, e.g., Wark and Fleming 1966),

$$R(\nu) = B(T_s,\nu)\,\tau(p_s,\nu) - \int_1^{\tau(p_s,\nu)} B(T(p),\nu)\,d\tau(p,\nu), \qquad (1)$$

where B = Planck radiance,
T = atmospheric temperature,
s = subscript indicating that a quantity is to be evaluated at the earth's surface,
p = atmospheric pressure, and
$\tau(p,\nu)$ = transmittance between the satellite and the level of the atmosphere with pressure p.

The Planck radiance is given by

$$B(T,\nu) = \frac{2hc^2\nu^3}{\exp[hc\nu/kT] - 1},$$

where h, c, and k are, respectively, Planck's constant, the speed of light, and Boltzmann's constant.

Equation (1) holds under cloudless conditions for nonscattering, plane-parallel atmospheres in local thermodynamic equilibrium.

2.2 Radiance Calculations in Wide Spectral Intervals

Equation (1) holds only for monochromatic radiation. For it to be applied to a spectral interval of a broad-band instrument, it must be convoluted with the spectral response function $\phi(\nu)$ of the interval. Figures 1 and 2 show such functions for channels 4 and 3 of the AVHRR on TIROS-N. The radiance R_ϕ that would be measured in any of these intervals is then given by

$$R_\phi = \int_0^\infty R(\nu)\,\phi(\nu)d\nu \Big/ \int_0^\infty \phi(\nu)d\nu, \qquad (2)$$

where $R(\nu)$ is computed from equation (1). To integrate equation (2) numerically, one must first integrate equation (1) numerically for a large number of closely spaced values of ν. This is too cumbersome for our purposes. However, if the function $\phi(\nu)$ is narrow enough (say, 30 cm^{-1} or less in half-width), we can find a wavenumber ν_o such that R_ϕ can be approximated adequately (Wark and Fleming 1966) by

$$R_\phi = B(T_s,\nu_o)\ \tau(p_s,\nu_o) - \int_1^{\tau(p_s,\nu_o)} B(T(p),\nu_o)\ d\tau(p,\nu_o), \qquad (3a)$$

where

$$\tau(p,\nu_o) = \int_o^\infty \tau(p,\nu)\ \phi(\nu)d\nu \ \Big/ \int_o^\infty \phi(\nu)d\nu\ . \qquad (3b)$$

Unfortunately, we are working with spectral intervals having widths of 100 cm^{-1} or greater, for which eq. (3) produces errors comparable to or exceeding the noise in the measurements of R_ϕ. We resort, then, to a more accurate procedure. We first subdivide each spectral interval into rectangular subintervals, 30 or 20 cm^{-1} in width, as shown in figures 3 and 4. Within these subintervals eq. (3) is an adequate approximation (see below); i.e., if the index i labels each subinterval, we can apply eq. (3) to compute a value of radiance R_i in the subinterval. Then to estimate the radiance for the full interval, we compute the weighted mean of the R_i's, where the weights are the heights h_i shown in figures 3 and 4. That is,

$$R_\phi = \sum_i h_i R_i \Big/ \sum_i h_i\ . \qquad (4)$$

In our calculations we chose the ν_o's to be at the center of each subinterval, and we chose the h_i's so that in each subinterval the area under the spectral response function equals the area of the rectangle. As shown in figures 3 and 4, the widths of the subintervals are 30 cm^{-1} near 11 μm and 20 cm^{-1} in the 3.7-μm region.

The accuracy of eq. (4) depends on the behavior of not only the Planck radiance, but also the transmittance, as functions of wavenumber in the spectral interval of interest. A simple, rough way to estimate the accuracy of eq. (4) is to ignore the transmittances, i.e., work with blackbody radiances instead of atmospheric radiances. Following this approach, for fixed temperature T we computed the blackbody radiances in three separate ways, the "exact" calculation and two approximations. For the exact calculation, we convoluted the Planck function $B(T,\nu)$ with the spectral response function, i.e., we applied eq. (2) with $R(\nu)$ replaced by $B(T,\nu)$. In numerically evaluating the integrals we applied the trapezoidal rule on points spaced every 0.1 cm^{-1}. The first approximation was simply the Planck function evaluated at the centroid of the spectral response function. (This is the form of eq. (3) for blackbody radiances.) For the spectral response functions shown in figures 1 and 2, the centroids are at 913.3 cm^{-1} and 2656.3 cm^{-1}, respectively. The second approximation was the one of eq. (4),

with R_i replaced by $B(T,\nu)$. The errors in each approximation were computed as the differences between the results of the approximations and those of the "exact" calculation. The absolute values of these errors are shown in figure 5 as functions of temperature. The upper panel applies to the AVHRR's 11-μm channel, and the lower to the AVHRR's 3.7-μm channel. The horizontal dashed lines are the nominal values of the NEΔN's (instrument noise, in radiance units) in the two channels. At 11 μm, the first approximation (centroid) produces errors comparable in magnitude to the NEΔN, while the second approximation (eq. (4)) holds the errors to values less than half of the NEΔN. At 3.7 μm, the first approximation (centroid) produces errors many times larger than the NEΔN, while eq. (4) reduces these errors to values approximately equal to the NEΔN. However, since we have ignored the transmittances in this analysis, the results provide only an estimate of the errors.

In the remainder of this report, eq. (4) is used in computations of atmospheric radiances.

2.3 Conversion of Atmospheric Radiances to Brightness Temperatures

In many applications, users of satellite data prefer to work with equivalent brightness temperature rather than radiance. We convert our calculated atmospheric radiances to brightness temperatures through look-up tables, one for each channel. Each table consists of 1501 pairs of blackbody radiances and their corresponding temperatures. The pairs are specified every 0.1°K between 180°K and 330°K. Each value of blackbody radiance in a table depends upon the spectral response function ϕ and is computed from eq. (4), with R_i replaced by $B(T,\nu_o)$. In other words, it is the weighted average of Planck radiances evaluated at the centers of the rectangular subintervals of figures 3 or 4, with the weights given by the heights h_i. The data in the look-up tables for channels 3 and 4 of the AVHRR are graphed in figure 6.

It is important to realize that because they are computed from eq. (4), the blackbody radiances in the look-up tables are not error-free, but carry with them the errors shown in figure 5. However, by computing the look-up table this way, we tend to minimize the errors in the inferred equivalent brightness temperatures, for the following reason: Recall that the first step in deriving an equivalent brightness temperature is the application of eqs. (3) and (4) to the atmospheric temperature profile to produce an atmospheric radiance. As previously described, this radiance carries with it an error than can be estimated from figure 5. The second step is to refer to this value of radiance in the look-up table and extract the corresponding equivalent brightness temperature. If the blackbody radiances in the look-up table are subject to exactly the same errors as are the atmospheric radiances, the errors in the two steps will compensate, and the derived equivalent brightness temperatures will be error-free. As described earlier, however, the errors in the blackbody radiances will not coincide exactly with the errors in the atmospheric radiances. Hence, using the look-up table generated from eq. (4), we will minimize the errors in the inferred equivalent brightness temperatures but not eliminate them.

3. CALCULATIONS OF TRANSMITTANCES

3.1 General

The first step in calculating radiances is to generate transmittances in each of the subintervals shown in figures 3 and 4. In the 11-μm window, eight intervals, each 30 cm^{-1} wide, span the region from 760 to 1000 cm^{-1}. In the 3.7-μm window, 23 intervals, each 20 cm^{-1} wide, span the region from 2440 to 2900 cm^{-1}. In each subinterval, the transmittance of the atmosphere is treated as a product of the transmittances of the atmospheric constituents that absorb radiation. In the 11-μm region, the constituents are water vapor and the "uniformly mixed gases" (McClatchey et al., 1972), principally carbon dioxide. In the 3.7-μm region, the constituents are water vapor, molecular nitrogen, and the uniformly mixed gases, chiefly carbon dioxide, nitrous oxide, and methane. We have intentionally neglected ozone. It is important only between 980 and 1000 cm^{-1}, whereas the responses of our satellite instruments, as measured by the $\phi(\nu)$ functions, are small, if not zero, in this subinterval. The effects of aerosols and clouds are also ignored.

3.2 Atmospheric Absorption Spectra

The purpose of this section is to describe generally the nature of atmospheric absorption in the window regions. Figures 7 and 8 are measured absorption spectra of the atmosphere in the 11- and 3.7-μm regions, respectively (Weinreb, Planet, and Jones 1977). (Figure 7 does not cover the entire 760-1000 cm^{-1} range, but it is useful, nonetheless, for the qualitative discussion here.) The spectra were taken with a spectrometer receiving solar radiation through the McMath solar telescope at the Kitt Peak National Observatory. The spectral resolution is about 0.7 cm^{-1} near 11 μm, and 7.0 cm^{-1} near 3.7 μm.

In the 11-μm window, water vapor dominates the absorption, contributing spectral lines and a continuum. The continuum (Bignell 1970) is absorption that has little dependence on wavenumber. In figure 7 its effect is most noticeable between the spectral lines, where the envelope of the spectrum has a value of transmittance less than one. In this case it is about 0.98, so the continuum absorption is about 2%. Incidentially, this spectrum was taken under very dry conditions (precipitable water = 0.6 cm). Under typical mid-latitude or tropical conditions (precipitable water $\approx$ 2 or 6 cm, respectively), the absorption is considerably stronger. For wavenumbers lower than 820 cm^{-1}, carbon dioxide makes some contribution to the absorption. Its effect is seen in the strong line near 792 cm^{-1} and in the background absorption that increases with decreasing wavenumber. Carbon dioxide also has a small effect between 930 and 1000 cm^{-1} (not shown in figure 7). As mentioned in the preceding section, our calculations ignore the absorption by ozone, which is measurable only for $\nu > 980$ cm^{-1}.

In the 3.7-μm window, the principal absorbers are nitrous oxide, carbon dioxide, methane, water vapor (mostly as HDO), and molecular nitrogen. Nitrous oxide contributes the band near 2570 cm^{-1} and the high-wavenumber part of the sharp fall-off between 2400 and 2500 cm^{-1}. Near 2400 cm^{-1} carbon dioxide dominates, but it rapidly loses strength toward higher wavenumbers. The region between 2400 and 2500 cm^{-1} is also affected by the collision-induced nitrogen absorption (Shapiro and Gush 1966, and Farmer and Houghton 1966). Between 2700 and 2900 cm^{-1}, water vapor and methane are the principal absorbers. Throughout the 3.7-μm window there is also a small contribution from the water-vapor continuum (White et al. 1978).

3.3 Transmittance of Atmospheric Constituents

3.3.1 Water Vapor

The transmittance of water vapor in the rectangular subintervals is treated as a product of the transmittances of spectral lines and of continua. For calculating transmittances of spectral lines, we use the method of Weinreb and Neuendorffer (1973). This method demands far less time and memory on the computer than does the line-by-line technique, yet it is nearly as accurate. The method treats the atmosphere as a succession of homogeneous layers, in each of which the pressure, temperature, and mixing ratio are constant. Over the path between the satellite and the bottom of a given layer, the transmittance τ_ℓ is computed from a function of the layer's total pressure (P) and temperature (T), and a scaled value of the water vapor amount (U). For the function of P, T, and U we chose a polynomial representation similar to that suggested by Smith (1969). In our calculation we used the following polynomial expression:

$$\ln(-\ln\tau_\ell) = \sum_{i=1}^{14} C_i(\nu)\, X_i \quad ,$$

where τ_ℓ is transmittance averaged over the rectangular subinterval,

$$X_1 = 1, \qquad X_2 = 0.1 \ln (UT/273), \qquad X_3 = \ln(P/1000),$$

$$X_4 = \ln(T/273), \qquad X_5 = X_2X_3, \qquad X_6 = X_2X_4 ,$$

$$X_7 = X_2^2 , \qquad X_8 = X_4X_7 , \qquad X_9 = X_3X_4,$$

$$X_{10} = X_2X_7, \quad X_{11} = X_4X_6 , \qquad X_{12} = X_4^2 ,$$

$$X_{13} = X_3X_6, \text{ and } X_{14} = X_3X_7.$$

The polynomial coefficients C_i were derived by a least-squares fitting of the polynomial to transmittances calculated line by line (Neuendorffer 1977) and averaged over the rectangular subintervals for a large dependent sample of homogeneous paths. Table 1 lists these coefficients.

The heart of the approximation is the procedure for calculating the scaled values of U in each layer. This is described in detail by Weinreb and Neuendorffer (1973).

The two water vapor continua are usually termed the self-broadened and the foreign-broadened continua. In the former, the absorption coefficient is proportional to the partial pressure of water vapor, while in the latter it is proportional to the partial pressure of the dry atmosphere. Following Roberts et al. (1976), the atmospheric transmittance in the self-broadened continuum is given by the equation,

$$-\ln \tau_{sb}(L,\nu) = C^{o}(\nu) \int_{o}^{L} W_{H_2O} P_{H_2O} \exp[T_o(\frac{1}{T} - \frac{1}{296})]d\ell \ , \qquad (5)$$

where $\tau_{sb}(L,\nu)$ = transmittance between the satellite and a level in the atmosphere at a distance L cm from the satellite,
W_{H_2O} = density of water vapor, in molecules cm^{-3},
P_{H_2O} = partial pressure of water vapor, in atmospheres,
T_o = reference temperature described below, and
$C^{o}(\nu)$ = coefficient described below.

For convenience in computation we have applied the hydrostatic equation to eq. (5) and made some changes in units to obtain

$$-\ln \tau_{sb}(P,\nu) = 5.41\text{x}10^{13} C^{o}(\nu) \sec\theta \int_{o}^{P} p\, r^2 \exp[T_o(\frac{1}{T} - \frac{1}{296})]dp, \qquad (6)$$

where θ = angle between line of sight and the local vertical,
P = atmospheric pressure in mb,
r = mass mixing ratio of water vapor in g/kg, and
$\tau_{sb}(P,\nu)$ = transmittance between the satellite and a point in the atmosphere with pressure P.

The values of C^{o} in eq. (6) are listed in table 2. For the 11-μm region, these values were derived from Roberts et al. (1976). For the 3.7-μm region they came from Burch et al. (1971). For T_o we use 1800°K in the 11-μm region, (Roberts et al. 1976), and in the 3.7-μm region we use the value of 1300°K, which was derived from the data of Burch et al. (1971).

The foreign-broadened continuum was ignored in the 11 μm region, because its effect is reported to be negligible (Roberts et al. 1976). In the 3.7-μm region, however, it cannot be ignored. The transmittance τ_f for this continuum is given by (Burch 1971),

$$-\ln \tau_f(L,\nu) = \gamma\, C^o(\nu) \int_o^L W_{H_2O}\, P_D\, d\ell \ . \qquad (7)$$

The notation in eq. (7) is the same as in eq. (5). Also, P_D is the partial pressure of the dry atmosphere, and γ is the ratio of foreign broadening to self-broadening. Equation (7) contains no temperature dependence, in part because it is poorly known, and in part because it is small.

As suggested by Burch et al. (1971) we adopted the value 0.12 for γ. Inserting this into eq. (7), using the approximation P_D = total pressure, and manipulating eq. (7) as we did eq. (5), we obtain

$$-\ln \tau_f\,(P,\nu) = 4.04\text{x}10^{15}\ \ C^o(\nu)\ \sec\theta \int_o^P p\ r\ dp. \qquad (8)$$

Note that the coefficients $C^o(\nu)$ have been selected at the centers of the subintervals of figures 3 and 4. Since these coefficients are slowly varying functions of wavenumber, the transmittances calculated from them are representative of averages over the subintervals of figures 3 and 4.

We have discussed separately the methods of calculation of transmittances for water vapor in spectral lines and the two continua. To obtain the overall transmittance of water vapor, we take the product of the transmittances of these three components.

3.3.2 Molecular Nitrogen

Molecular nitrogen has a collision-induced absorption band centered at 2330 cm^{-1}. Following Burch et al. (1971), the transmittance τ_N in this band for homogeneous paths (paths where pressure, temperature, and mixing ratios are all constant), is given by,

$$-\ln \tau_N(L,\nu) = 5.67\text{x}10^{26}\ \ C_N(T,\nu)\ \ \frac{P_A^2\, L}{T}\ , \qquad (9)$$

where P_A = atmospheric pressure in atmospheres, and $C_N(T,\nu)$ = Burch's "self-induced" coefficient for nitrogen absorption, in units of $molecules^{-1}\ cm^2\ atm^{-1}$. The remaining notation is as in eq. (5).

The coefficient $C_N(T,\nu)$ has a pronounced dependence on temperature, which is formulated as follows: Susskind and Searl (1977) demonstrate that the quantity $\frac{\ln \tau_N}{\rho^2 L}$ is very nearly independent of T, where ρ is number density of N_2 in units of molecules cm^{-3}. By combining eq. (9) with the hydrostatic equation, we get

$$C_N(T,\nu) \sim \frac{\ln \tau_N(L,\nu)}{\rho^2 L\, T} \quad .$$

Therefore, $C_N(T,\nu)$ has a temperature dependence of $\frac{1}{T}$, and we can define a temperature-independent coefficient $C_N(296,\nu)$ by

$$C_N(296,\nu) = \frac{T}{296} C_N(T,\nu) \quad . \tag{10}$$

Combining eqs. (9) and (10) and applying the result to an atmospheric slant path, we obtain

$$-\ln \tau_N(L,\nu) = 5.67\text{x}10^{26}\, C_N(296,\nu) \int_0^L \left(\frac{296}{T}\right) \frac{P_A^2}{T}\, d\ell. \tag{11}$$

Manipulating eq. (11) as we did eq. (5), we obtain the form used in our computations,

$$-\ln \tau_N(P,\nu) = 4.77\text{x}10^{21}\, C_N(296,\nu)\, \sec\theta \int_0^P p/T\, dp. \tag{12}$$

The coefficients $C_N(296,\nu)$ were derived from Shapiro and Gush (1966) and are given in the fourth column of table 2. Since they are slowly varying functions of wavenumber, the transmittances calculated from them are representative of averages over the subintervals of figures 3 and 4.

3.3.3 Uniformly mixed gases

The uniformly-mixed gases comprise CO_2, N_2O, CO, CH_4, and O_2. As mentioned in section 3.2, CO_2 absorbs weakly in the 11-μm window, whereas CO_2, N_2O and CH_4 absorb weakly in the 3.7-μm window. The method of calculating transmittances is taken from LOWTRAN (McClatchey et al. 1972 and Selby et al. 1978) and is summarized in the following paragraphs.

The transmittances from LOWTRAN have a spectral resolution of 20 cm^{-1} and are specified at every 5 cm^{-1} throughout the visible and infrared spectrum. Transmittances are computed separately for each of the processes in the atmosphere, e.g., absorption by uniformly mixed gases, absorption by water vapor continua, molecular scattering, etc. The uniformly mixed gases are treated as a unit, with relative concentrations given in McClatchey et al. (1972). These concentrations are built into the model, so that the user does not have to specify them. The basic idea of LOWTRAN is that transmittances through any slant path can be calculated rapidly in a single operation by the equation,

$$\tau_u(\nu, P, T) = F\left[C_u(\nu) + \log_{10}\omega(P,T)\right], \tag{13}$$

where τ_u = transmittance of the uniformly mixed gases,
$C_u(\nu)$ = wavenumber-dependent coefficient, related to the absorption coefficient representing a 20 cm^{-1} interval,
ω = "equivalent absorber amount" in the slant path, and
F = a known function, specified in a look-up table, as described below.

LOWTRAN applies eq. (13) in calculations of transmittances for all molecular species. However, the following material, which describes the variable ω and the coefficient $C_u(\nu)$, applies only to the uniformly mixed gases.

The "equivalent absorber amount" ω, between an atmospheric layer at altitude Z (km) and the satellite, is given by

$$\omega = \sec\theta \int_Z^\infty \left(\frac{P}{Po}\right)^{7/4}\left(\frac{T_o}{T}\right)^{11/8} dz, \tag{14}$$

where T_o and Po are standard temperature and pressure (273.15°K and 1013 mb in LOWTRAN).

Manipulating eq. (14) as we did eq. (5), we obtain the form used in our computations,

$$\omega = 7.89\text{x}10^{-3}\sec\theta \int_o^P \left[\frac{p}{p_o}\left(\frac{T_o}{T}\right)^{1/2}\right]^{3/4} dp, \tag{15}$$

where the notation is the same as in eq. (6).

The wavenumber-dependent coefficients $C_u(\nu)$, taken from Selby et al. (1978), are listed in table 2.

For convenience in describing the function F, we define its argument to be β, i.e.,

$$\beta \equiv C_u(\nu) + \log_{10} \omega(P,T).$$

The argument β is evaluated by the procedures already described. The final step in determining τ_u is to use the look-up table relating β to τ_u. In figure 9 this relation is graphed over the part of its domain that corresponds to $.900 \leq \tau \leq .999$. This range covers the values of transmittance that are encountered in the 3.7- and 11-μm windows for the vertical or nearly vertical paths considered here. As an example of the use of the look-up table, figure 9 shows that if one enters a value of -0.5 for β, he finds a value of approximately 0.97 for τ_u. Since the values of transmittance derived in this way are averages over 20-cm^{-1} intervals, they can be applied directly in the 20-cm^{-1} rectangular subintervals in the 3.7-μm window. In the 11-μm window, we used the 20-cm^{-1} averages for LOWTRAN to represent the transmittances in the 30-cm^{-1} wide rectangular subintervals. Since the absorption is small and varying slowly with wavenumber, we are confident that this additional approximation is permissible.

4. COMPUTATIONAL DETAILS AND RESULTS

4.1 Quadrature

The computations of transmittances employ eqs. (6), (8), (12), and (15), which involve integrals with respect to atmospheric pressure. In numerically evaluating these integrals, we apply the trapezoidal rule on the 100 quadrature points listed in table 3. These points represent equal increments on the scale of $P^{2/7}$.

In computing radiances we evaluate eq. (3a) by the trapezoidal rule, specifying B and τ at the 100 quadrature points listed in table 3. Because the transmittances are already averages over the rectangular subintervals of figures 3 and 4, as discussed in the previous section, we do not use eq. (3b). As also discussed previously, the wide-band radiances are computed from eq. (4), and brightness temperatures are inferred from the look-up table as illustrated in figure 6.

With the 100 quadrature points of table 3, we can most conveniently compute radiances for those atmospheres that have their surface pressure equal to 1000 mb. However, the computer program that performs these calculations can also handle atmospheres with surface pressures different from 1000 mb. If the surface has a pressure greater than 1000 mb, we simply include that level in all the integrations as a 101st quadrature point. On the other hand, if the surface has a pressure less than 1000 mb, we retain all 100 quadrature levels in the integrations. However, to all levels whose pressures exceed the surface pressure, we assign a value of temperature equal to the surface temperature and a value of mixing ratio equal to the mixing ratio at the surface. Also, in eq. (3a) the surface term is placed at the 1000 mb level. The radiances that are computed by this procedure are identical to the

radiances that would have been computed if we had integrated from the top of the atmosphere down only as far as the actual surface.

For completeness we should also mention that the computer program is designed to use two values of temperature at the surface; one to represent the radiative temperature of the surface itself (T_S), and the second to represent the temperature of the atmosphere at the surface (the shelter temperature), e.g. the value of T at P = 1000 mb. Often, however, atmospheres are provided without a value of T_S being specified. In that case the program automatically picks a value of T_S equal to the shelter temperature.

4.2 Examples

4.2.1 Atmospheres

All calculations were done for the three atmospheres whose temperature profiles are shown in figure 10, and whose profiles of water-vapor mixing ratio are shown in figure 11. They represent a diversity of conditions. All three of these examples have P = 1000 mb at the earth's surface.

4.2.2. Transmittances

Figures 12 and 13 show transmittances calculated in each of the sub-intervals in the 11- and 3.7-μm windows, respectively, for water-vapor, nitrogen, and the uniformly-mixed gases. The AVHRR spectral response functions also appear in these figures. In figure 12 the water-vapor transmittances were calculated for two atmospheres -- 64°N, labelled "dry" (total precipitable water = 0.75 cm), and 9°N, labelled "moist" (total precipitable water = 4.86 cm). The absorption by the uniformly mixed gases is unchanged for the two atmospheres. Not only is water vapor the strongest absorber in this spectral region, but it is also the most variable. In figure 13 the transmittances were calculated for only the moist (9°N) atmosphere. Since the absorption is weak in this region of the spectrum, its variability from wet to dry is less than that observed at 11 μm. In any case, water vapor is the principal absorber for wavenumbers higher than about 2600 cm^{-1}. Below 2600 cm^{-1}, the nitrogen collision-induced absorption is of significance, and it becomes dominant below 2500 cm^{-1}.

4.2.3 Atmospheric Attenuation

Atmospheric attenuation is used here to mean the difference between the earth's surface temperature and the brightness temperature measured at the satellite. This quantity is of interest because one of the major applications of data from satellite-borne radiometers is in determining surface temperature. In operational sounding we seldom have available the atmospheric temperature and humidity profiles necessary to calculate attenuation by the method of this report. However, these calculations are useful for simulations and for case studies, where data from both the satellite radiometer and concurrent radiosondes are available.

Figure 14 shows the variation of attenuation with total precipitable water in the atmosphere for a vertical path ($\sec\theta = 1$). The calculations were done for the AVHRR's channel 4 (lower panel) and channel 3 (upper panel). In all calculations the surface temperatures were set equal to the temperatures at 1000 mb. Calculations were done separately for each of the three atmospheres of figures 10 and 11. We varied the total precipitable water by multiplying the mixing ratio profiles from figure 10 by 0.1, 0.2, 0.5, 1, 2, 3, and 4. However, the mixing-ratios were never allowed to exceed values at saturation.

As expected, the attenuation at 11 μm is a stronger function of precipitable water than is the attenuation at 3.7 μm. One interesting result is that for precipitable water less than about 2 cm, the attenuation is greater at 3.7 μm than it is at 11 μm, while for the higher water vapor amounts the reverse is true. This is a consequence of the fact that water vapor is the major absorber in one interval, while the uniformly mixed gases and nitrogen predominate in the other.

Figure 15 illustrates a second, perhaps more realistic, approach to demonstrate the dependence of attenuation on total precipitable water in the 11-μm window. The data in this figure were compiled by E.P. McClain (1979) from a set of 60 atmospheres representing a range of typical maritime conditions around the globe. From our computer program, he obtained the attenuation in a vertical path for each atmosphere, and these are plotted as the +'s in the figure. Incidentially, in all calculations, he set the surface temperatures equal to the temperatures at 1000 mb. The solid lines in the figure are the data from figure 14, which are included for the purpose of comparison.

Figures 16 and 17 show the variation of attenuation with surface temperature for channels 4 and 3, respectively, for vertical paths. These calculations were also done separately for each of the three atmospheres. In each, we varied the surface temperature about the 1000 mb value given in figure 10 by $0^{\circ}K$, $\pm 3^{\circ}K$, $\pm 6^{\circ}K$, $\pm 9^{\circ}K$, and $\pm 12^{\circ}K$. The arrows indicate the temperature at 1000 mb for each atmosphere.

5. CONCLUSION

The method described here enables us to calculate atmospheric radiances, brightness temperatures, and attenuations in the wide spectral intervals of satellite radiometers in the 3.7- and 11-μm windows. The method involves integrating the radiative transfer equation. Because transmittances are modelled rather than computed line by line, the calculations are rapid. As input, the method requires vertical profiles of atmospheric temperature and water-vapor mixing ratio. Hence its main utility is in case studies and simulations, not in real-time retrievals of surface temperatures from satellite data.

We are better able to estimate the accuracy of the calculations at 11 μm than at 3.7 μm. Since we have considerable experience (dating back to the SIRS instruments on the Nimbus 3 and 4 satellites in the late 1960s) with calculations and measurements at 11 μm, we feel that these calculations are not grossly in error. The error is probably less than 1 $mW/(m^2\ sr\ cm^{-1})$. However, at 3.7 μm we have little experience, and we are not in a position to offer an estimate of accuracy. There is a need for work on the absorption properties of atmospheric gases in this spectral region. In addition, studies comparing measurements with the calculations have yet to be carried out.

The method described here is incorporated in a computer program that is available by writing to the authors.

ACKNOWLEDGMENTS

The authors thank A.C. Neuendorffer of NESS for computing the polynomial coefficients in table 1, E. P. McClain of NESS for supplying data in figure 16, and Kay Collins for preparing the manuscript.

REFERENCES

Anding, D. and R. Kauth, 1969: Atmospheric modelling in the infrared spectral region: atmospheric effects on miltispectral sensing of sea-surface temperatures from space. Report 2676-1-P, Willow Run Laboratories, Institute of Science and Technology, The University of Michigan, Ann Arbor, MI.

Bignell, K.J., 1970: The water vapour infra-red continuum. Quant. J. R. Met. Soc., 96, 390-403.

Burch, D.E., D.A. Gryvnak, and J.D. Pembrook, 1971: Investigation of the absorption of infrared radiation by atmospheric gases: water, nitrogen, nitrous oxide. Semi-Annual Technical Report. No. 2, AFCRL-71-0124, Philco-Ford Corporation, Aeronutronic Division, Newport Beach, CA, 25 pp.

Davis, P.A. and W. Viezee, 1964: A model for computing infrared transmission through atmospheric water vapor and carbon dioxide. J. Geophys. Res., 69, 3785-3794.

Farmer, C.B. and J.T. Houghton, 1966: Collison-induced absorption in the Earth's atmosphere. Nature, 209, 1341-1342.

Lauritson, Levin (National Environmental Satellite Service, National Oceanic and Atmospheric Administration, U.S. Department of Commerce, Washington, D.C.), 1979 (personal communication).

Maul, George A. and M. Sidran, 1973: Atmospheric effects on ocean surface temperature sensing from the NOAA satellite scanning radiometer. J. Geophys. Res., 78, 1909-1916.

McClain, E.P. (National Environmental Satellite Service, National Oceanic and Atmospheric Administration, U.S. Department of Commerce, Washington, D.C.), 1979 (personal communication).

McClatchey, Robert A., R.W. Fenn, J.E.A. Selby, F.E. Volz, and J.S. Garing, 1972: Optical properties of the atmosphere (third edition). AFCRL-72-0497, Air Force Cambridge Research Laboratories, L.G. Hanscom Field, Bedford, MA, 108 pp.

McClatchey, Robert A., W.S. Benedict, S.A. Clough, D.E. Burch, R.F. Calfee, K. Fox, L.S. Rothman, and J.S. Garing, 1973: AFCRL atmospheric absorption line parameters compilation. AFCRL-TR-73-0096, Air Force Cambridge Research Laboratories, L.G. Hanscom Field, Bedford, MA, 78 pp.

McMillin, L.M., D.Q. Wark, J.M. Siomkajlo, P.G. Abel, A. Werbowetski, L.A. Lauritson, J.A. Pritchard, D.S. Crosby, H.M. Woolf, R.C. Luebbe, M.P. Weinreb, H.E. Fleming, F.E. Bittner, and C.M. Hayden, 1973: Satellite infrared soundings from NOAA spacecraft. NOAA Technical Report NESS 65, National Oceanic and Atmospheric Administration, U.S. Department of Commerce, Washington, D.C. 112 pp.

Neuendorffer, A.C., 1977: Rapid atmospheric transmittance through fast Fourier convolution. J. Opt. Soc. Am., 67, 1376.

Roberts, Robert E., J.E.A. Selby, and L.M. Biberman, 1976: Infrared continuum absorption by atmospheric water vapor in the 8-12 μm window. Appl. Opt., 15, 2085-2090.

Saiedy F. and D.T. Hilleary, 1967: Remote sensing of surface and cloud temperatures using the 899 cm^{-1} interval. Appl. Opt., 6, 911-917.

Selby, J.E.A., F.X. Kneizys, J.H. Chetwynd, Jr., and R.A. McClatchey, 1978: Atmospheric transmittance/radiance: Computer code LOWTRAN 4. AFGL-TR-78-0053, Air Force Geophysics Laboratory, Hanscom AFB, Bedford, MA, 100 pp.

Shapiro, M.M. and H.P. Gush, 1966: The collision-induced fundamental and first overtone bands of oxygen and nitrogen. Can. J. Phys., 44, 949-963.

Smith, W.L. 1969: A polynomial representation of carbon dioxide and water vapor transmission. ESSA Technical Report NESC 47, Environmental Science Services Administration, U.S. Department of Commerce, Washington, D.C., 20 pp.

Smith, W.L., P.K. Rao, R. Koffler, and W.R. Curtis, 1970: The determination of sea-surface temperature from satellite high-resolution infrared window radiation measurements. Mon. Wea. Rev., 8, 604-611.

Susskind, J. and J.E. Searl, 1977: Atmospheric absorption near 2400 cm^{-1}. J. Quant. Spectrosc. Radiat. Transfer, 18, 581-587.

Wark, David Q., Yamamoto, G., and Lienesch, J.H., 1962: Methods of estimating infrared flux and surface temperature from meteorological satellites. J. Atmos. Sci., 19, 369-384.

Wark, David Q. and H.E. Fleming, 1966: Indirect measurements of atmospheric temperature profiles from satellites: 1. Introduction. Mon. Wea. Rev., 94, 351-362.

Wark, David Q., J.H. Lienesch, and M.P. Weinreb, 1974: Satellite observations of atmospheric water vapor. Appl. Opt., 13, 507-511.

Weinreb, Michael P. and A.C. Neuendorffer, 1973: Method to apply homogeneous-path transmittance models to inhomogeneous atmospheres. J. Atmos. Sci., 30, 662-666.

Weinreb, M.P., W.G. Planet, and G.D. Jones, 1977: Transmittance of the atmosphere to infrared solar radiation. J. Opt. Soc. Am., 67, 1377.

White, Kenneth O., W.R. Watkins, C.W. Bruce, R.E. Meredith, and F.G. Smith, 1978: Water vapor continuum absorption in the 3.5 - 4.0-μm region. Appl. Opt., 17, 2711-2720.

Blank page retained for pagination

Table 1.--Polynomial coefficients for spectral lines of water vapor

Subinterval	$\nu_o(cm^{-1})$*	C_1	C_2	C_3	C_4	C_5	C_6
1	775.0	-2.23135	6.12346	0.45051	2.71498	1.20255	-1.96786
2	805.0	-1.85030	5.82894	0.41698	2.97656	1.11404	-2.67401
3	835.0	-3.09180	7.02594	0.32994	3.39958	1.23004	-3.45263
4	865.0	-2.81430	6.57833	0.39086	3.97101	1.26900	-4.46690
5	895.0	-3.27104	7.08477	0.36451	3.99316	1.13824	-2.29048
6	925.0	-3.87608	7.84570	0.28824	5.04843	1.23165	-2.31676
7	955.0	-3.96672	7.95368	0.26595	4.60590	1.02471	-1.36628
8	985.0	-4.05978	8.80584	0.18746	5.10449	1.06154	-2.46299
9	2450.0	-8.43013	15.21933	0.60791	0.0	0.0	15.86929
10	2470.0	-8.72307	23.63057	0.0	0.0	0.0	0.0
11	2490.0	-6.99218	8.24594	0.0	0.0	0.0	38.69545
12	2510.0	-6.38534	8.55110	0.0	0.0	0.91916	35.69487
13	2530.0	-5.98694	9.68929	-0.17617	3.36765	0.0	2.67673
14	2550.0	-5.33819	9.31851	0.0	2.95701	0.0	0.0
15	2570.0	-4.24407	9.72573	0.0	1.91971	0.0	-0.94502
16	2590.0	-3.75231	9.61935	0.05234	1.04405	0.46435	-0.50525
17	2610.0	-3.24848	9.12599	0.06984	0.27549	0.57222	-0.48066
18	2630.0	-2.55092	8.73256	0.16667	-0.41303	1.24934	1.04954
19	2650.0	-2.62371	8.72498	0.18783	-0.92050	1.16865	1.31301
20	2670.0	-2.57342	8.50253	0.21895	-1.35674	1.28026	1.95386
21	2690.0	-3.01532	8.69507	0.13112	-1.49397	0.79516	1.75717
22	2710.0	-2.63606	9.24895	0.15824	-0.27694	0.80061	1.56005
23	2730.0	-2.07502	8.20344	0.12908	-1.29617	1.31776	1.96238
24	2750.0	-3.17113	8.81213	0.12185	-1.67030	0.65181	1.46866
25	2770.0	-2.57576	8.39041	0.19882	-1.78166	1.26947	1.64839
26	2790.0	-2.31882	8.75249	0.20187	-1.25449	1.13656	1.53516
27	2810.0	-2.29242	8.58541	0.17273	-0.74559	1.09597	1.18283
28	2830.0	-2.58936	9.27357	0.10902	-0.05086	0.83697	0.96999
29	2850.0	-3.20658	9.73757	0.02928	0.23195	0.32549	-0.47011
30	2870.0	-3.38421	9.50275	0.04329	0.74368	0.34426	-0.78017
31	2890.0	-3.36249	8.32141	0.18909	1.40180	0.59159	-2.23602

*Midpoint of subinterval

Table 1.--Polynomial coefficients for spectral lines of water vapor (continued)

Subinterval	C_7	C_8	C_9	C_{10}	C_{11}	C_{12}	C_{13}	C_{14}
1	-3.76620	0.16593	0.43179	3.83257	2.18960	-1.57369	3.31522	-1.34526
2	-3.92641	-2.77498	0.31976	2.79153	0.32945	-1.52147	3.42676	-1.05728
3	-6.40380	-1.00006	0.61283	5.99156	0.66930	-0.59443	7.08475	-4.82659
4	-5.74839	-0.50223	0.78782	6.00689	0.48105	-2.76763	7.00733	-4.61433
5	-5.69290	-0.64269	0.30803	7.74251	-2.16183	-0.78133	3.28952	-5.12407
6	-5.89552	-3.71300	0.36473	6.08009	-3.61897	-0.21804	6.03967	-4.22350
7	-4.72846	-3.68452	0.30339	5.13370	-1.26021	-0.67621	5.42607	-4.19546
8	-5.15066	-9.38148	0.43482	2.28616	0.52204	-2.57286	6.41268	-3.49313
9	-20.04587	0.0	-8.89374	20.63594	-116.74747	33.37996	0.0	0.0
10	-50.03848	36.53720	-10.09401	55.29951	-134.74405	40.28809	0.0	16.65234
11	2.24573	74.76546	0.0	0.0	0.0	0.0	0.0	5.02699
12	0.0	71.44127	0.0	5.61771	-35.20401	8.97379	-7.05114	0.0
13	4.28756	10.06262	0.0	-13.55549	-9.75042	0.0	0.0	9.83851
14	5.48571	-3.73073	0.0	-17.92360	0.0	-2.39925	0.0	4.49243
15	0.74369	-2.64936	0.0	-13.21884	0.0	-1.99500	0.0	6.24828
16	-1.28595	-2.82817	0.0	-10.27634	0.0	-1.52861	0.0	3.20704
17	-3.49510	-0.91434	0.0	-7.74922	0.0	-0.96192	0.0	1.88804
18	-6.33610	-3.22005	-0.00891	0.95724	0.0	-0.57106	3.56149	-3.29910
19	-5.87246	-3.23284	0.0	3.32840	0.0	-0.48695	3.61152	-3.90407
20	-6.16732	-2.35241	-0.09758	4.72198	0.0	0.0	3.52096	-4.33986
21	-3.80712	1.72189	-0.11658	-1.68104	0.0	0.0	0.0	1.11738
22	-4.91668	-3.52099	0.01092	0.41617	0.0	0.0	5.75246	-4.60047
23	-6.62488	0.0	-0.16732	1.01783	-2.43217	0.0	4.34945	-2.02269
24	-3.44052	1.19814	0.0	-1.70164	0.0	0.0	0.0	0.98203
25	-6.19237	0.0	-0.44376	4.41116	0.0	0.0	0.0	-3.59585
26	-5.86578	-2.40387	-0.15961	3.21334	0.0	0.0	2.97682	-4.05581
27	-5.80459	-3.41682	0.0	4.01662	0.0	-0.45678	3.43357	-3.93663
28	-4.70158	-6.29812	0.0	1.21437	0.0	0.0	5.65174	-3.46406
29	-1.50509	-0.80652	0.0	-6.04562	0.0	0.0	0.0	1.16613
30	-1.87255	0.0	0.0	-3.55467	0.0	0.85632	0.0	0.0
31	-2.62032	2.13675	0.22333	2.59861	2.14038	0.38428	0.0	-0.41753

Table 2.--Coefficients for water-vapor continuum, nitrogen absorption, and uniformly mixed gases

Subinterval	$\nu_o(cm^{-1})$*	$C^o(\nu)x10^{24}$ ($molec^{-1}cm^2atm^{-1}$)	$C_N(296,\nu)x10^{28}$ ($molec^{-1}cm^2atm^{-1}$)	$C_u(\nu)$
1	775	500		-0.53
2	805	421		-1.18
3	835	359		-2.51
4	865	310		-5.00
5	895	271		-5.00
6	925	240		-1.71
7	955	216		-1.11
8	985	197		-1.33
9	2450	4.30	323	-1.12
10	2470	3.95	240	-1.20
11	2490	3.65	164	-1.54
12	2510	3.40	99.9	-2.26
13	2530	3.15	64.6	-1.06
14	2550	2.90	47.0	-0.45
15	2570	2.75	29.4	-0.37
16	2590	2.70	23.5	-0.75
17	2610	2.70	17.6	-2.60
18	2630	2.75	5.88	-2.51
19	2650	2.95		-2.42
20	2670	3.20		-2.43
21	2690	3.45		-2.68
22	2710	3.70		-2.83
23	2730	4.00		-2.66
24	2750	4.35		-2.26
25	2770	4.65		-2.02
26	2790	5.00		-1.86
27	2810	5.35		-1.79
28	2830	5.70		-1.69
29	2850	6.05		-1.78
30	2870	6.40		-1.21
31	2890	6.80		-0.53

*Midpoint of subinterval

Table 3.--The 100 quadrature points for integrations over atmospheric pressure

Level	Pressure (mb)	Level	Pressure (mb)	Level	Pressure
1	.0100	35	30.2057	68	271.2454
2	.0225	36	33.0936	69	284.8863
3	.0435	37	36.1736	70	299.0103
4	.0756	38	39.4530	71	313.6276
5	.1220	39	42.9395	72	328.7482
6	.1858	40	46.6407	73	344.3825
7	.2704	41	50.5644	74	360.5409
8	.3795	42	54.7183	75	377.2336
9	.5169	43	59.1104	76	394.4712
10	.6866	44	63.7488	77	412.2642
11	.8928	45	68.6414	78	430.6233
12	1.1399	46	73.7966	79	449.5590
13	1.4323	47	79.2226	80	469.0821
14	1.7747	48	84.9277	81	489.2034
15	2.1719	49	90.9204	82	509.9338
16	2.6289	50	97.2092	83	531.2841
17	3.1507	51	103.8028	84	553.2655
18	3.7427	52	110.7098	85	575.8890
19	4.4101	53	117.9389	86	599.1656
20	5.1584	54	125.4991	87	623.1066
21	5.9934	55	133.3993	88	647.7232
22	6.9207	56	141.6485	89	673.0267
23	7.9462	57	150.2558	90	699.0285
24	9.0758	58	159.2303	91	725.7401
25	10.3158	59	168.5813	92	753.1729
26	11.6724	60	178.3181	93	781.3385
27	13.1517	61	188.4501	94	810.2486
28	14.7804	62	198.9869	95	839.9147
29	16.5050	63	209.9378	96	870.3487
30	18.3920	64	221.3126	97	901.5623
31	20.4284	65	233.1210	98	933.5674
32	22.6209	66	245.3727	99	966.3760
33	24.9766	67	258.0775	100	1000.0000
34	27.5025				

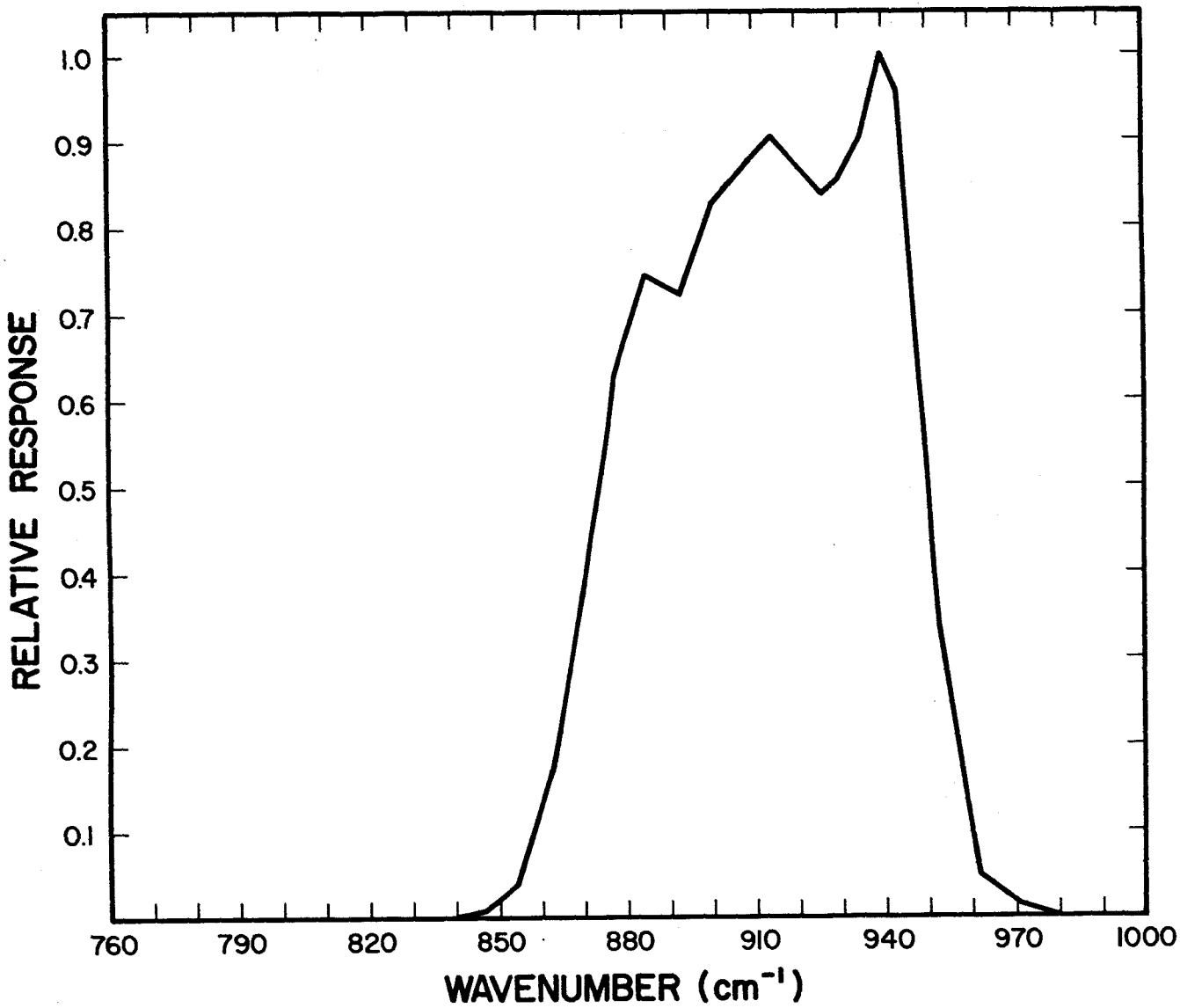

Figure 1.--Spectral response function for channel 4 of AVHRR on TIROS-N (Lauritson 1979).

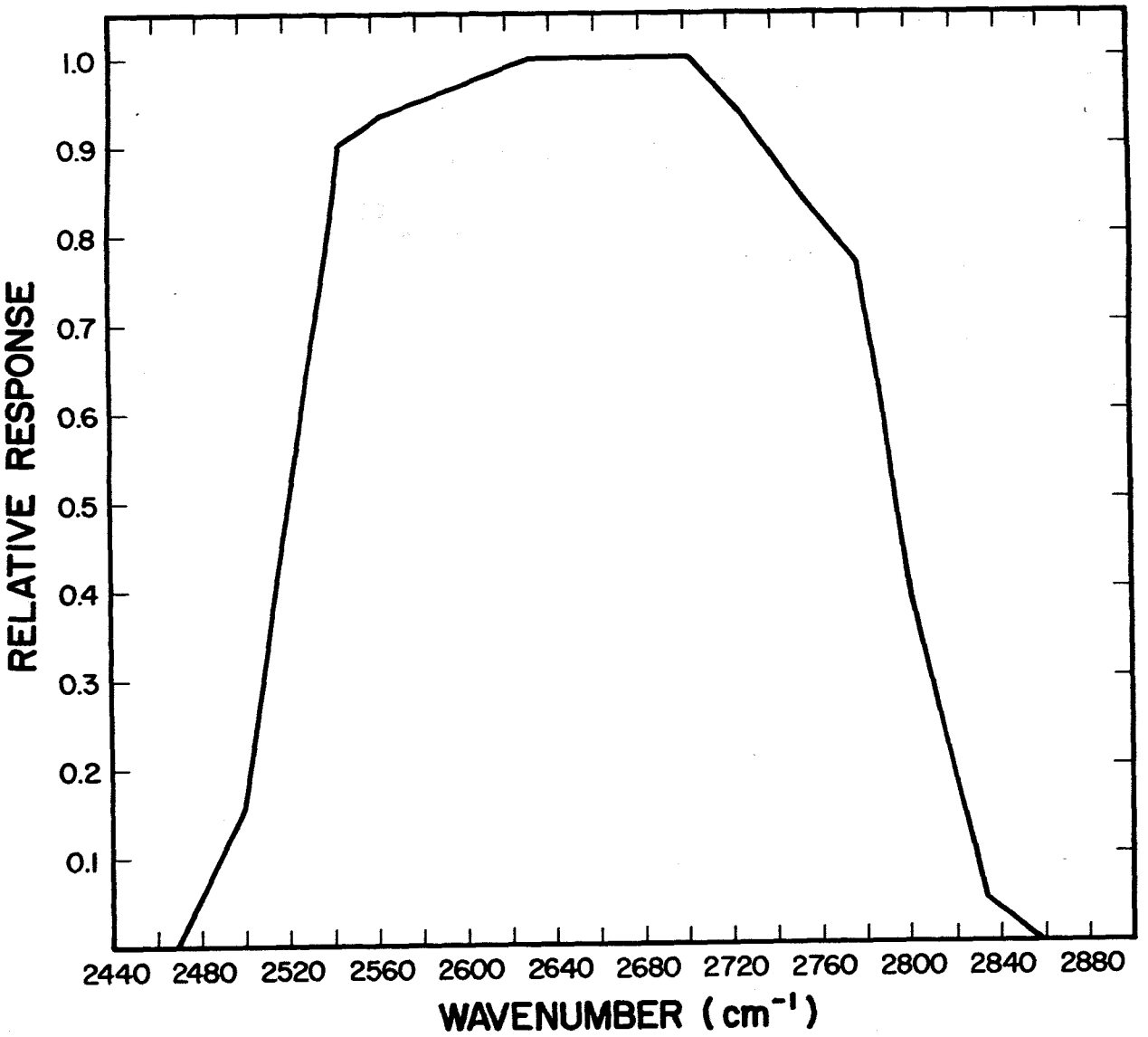

Figure 2.--As in figure 1, for channel 3.

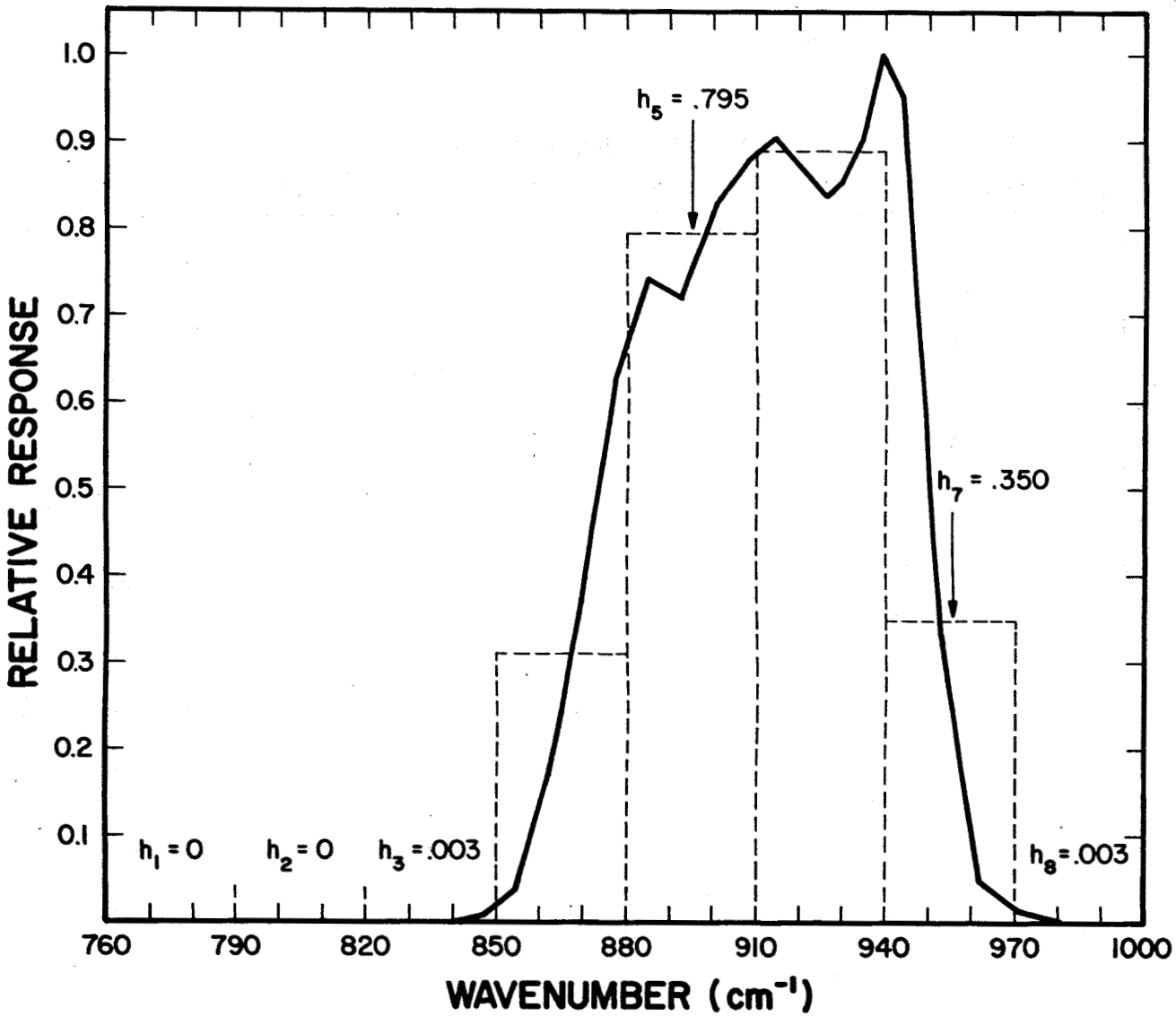

Figure 3.--Rectangular subintervals in region of channel 4 of AVHRR on TIROS-N.

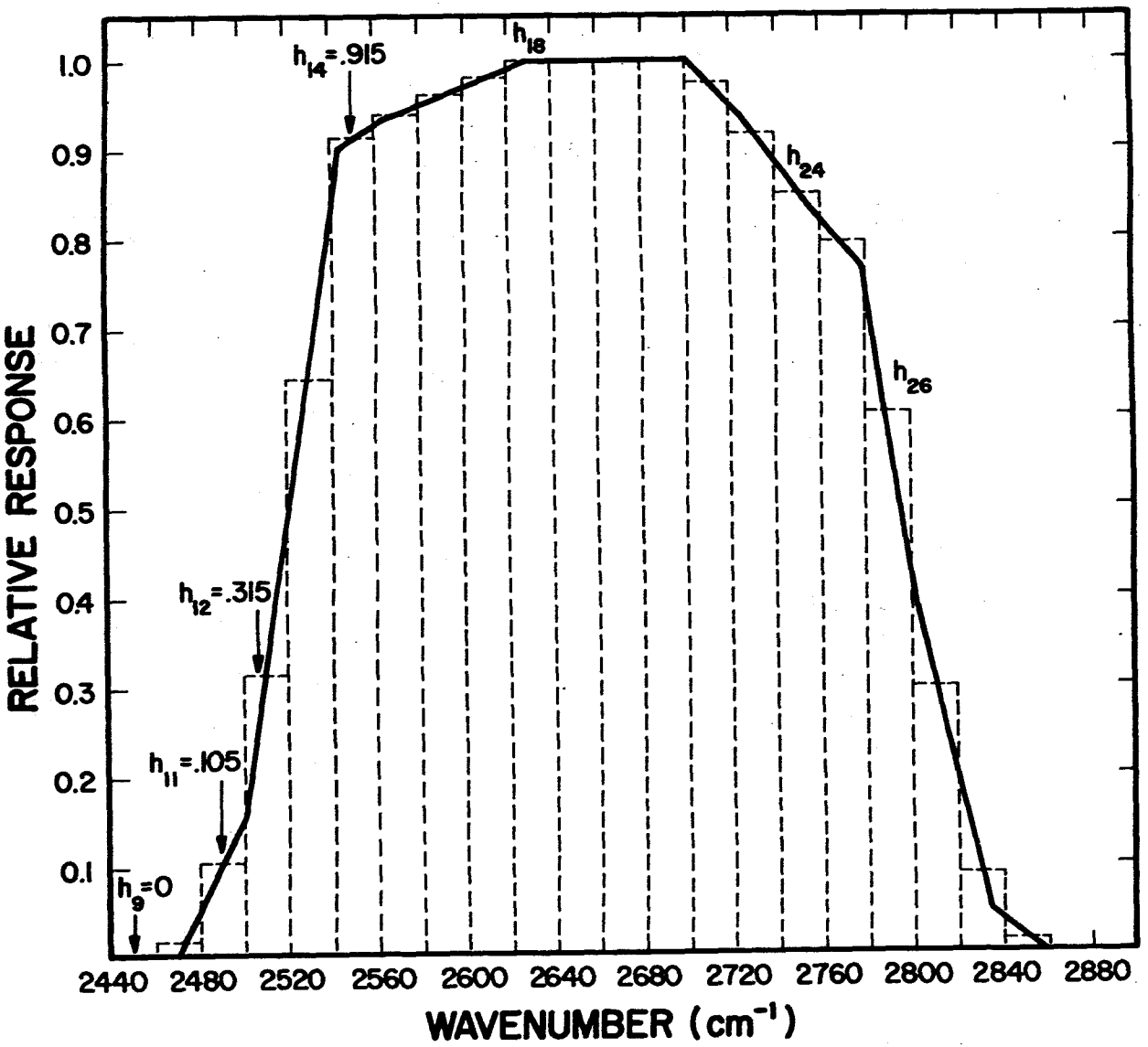

Figure 4.--As in figure 3, for channel 3

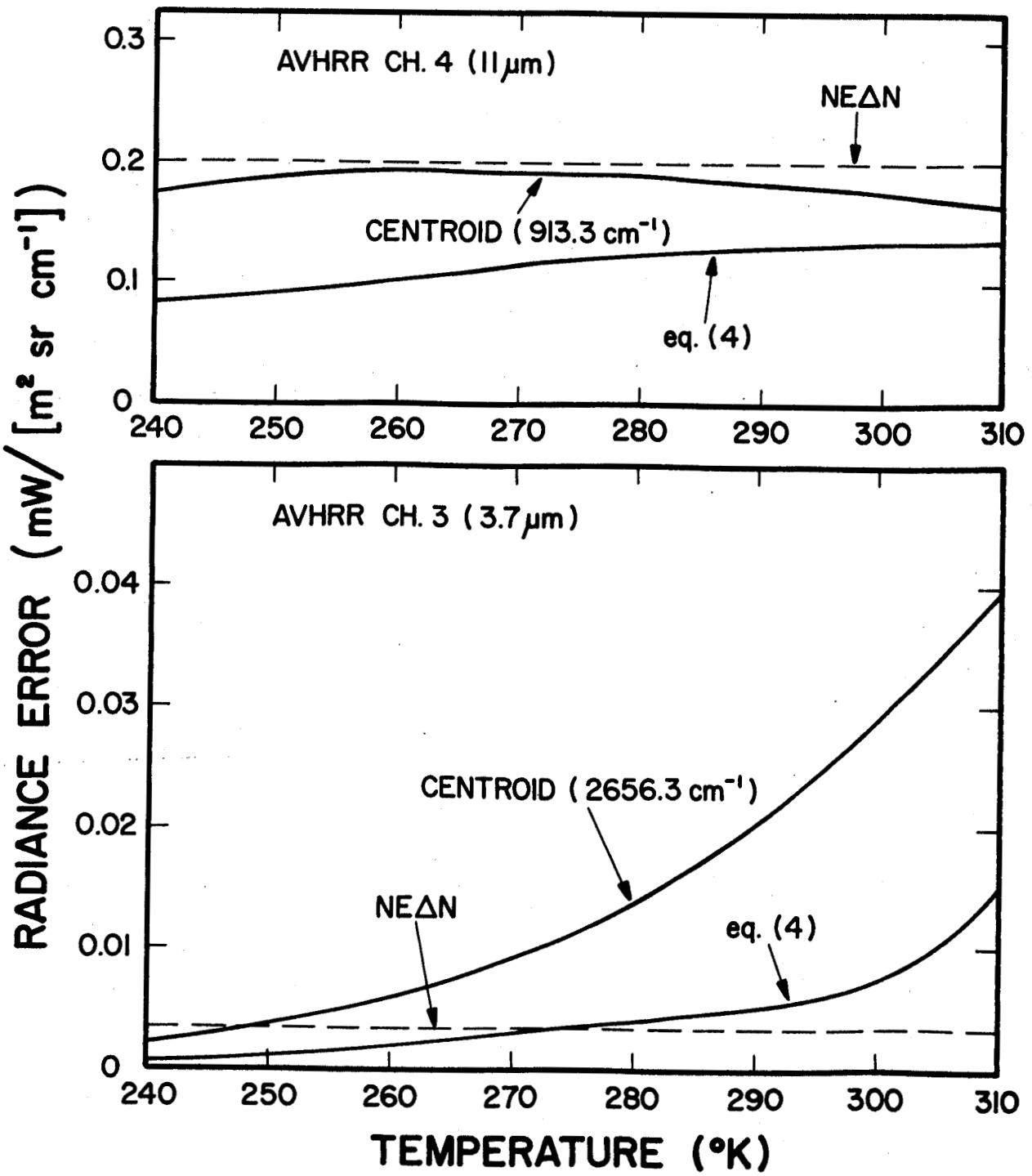

Figure 5.--Errors in calculated blackbody radiances vs temperature, for the "centroid" approximation and for the approximation of eq. 4.

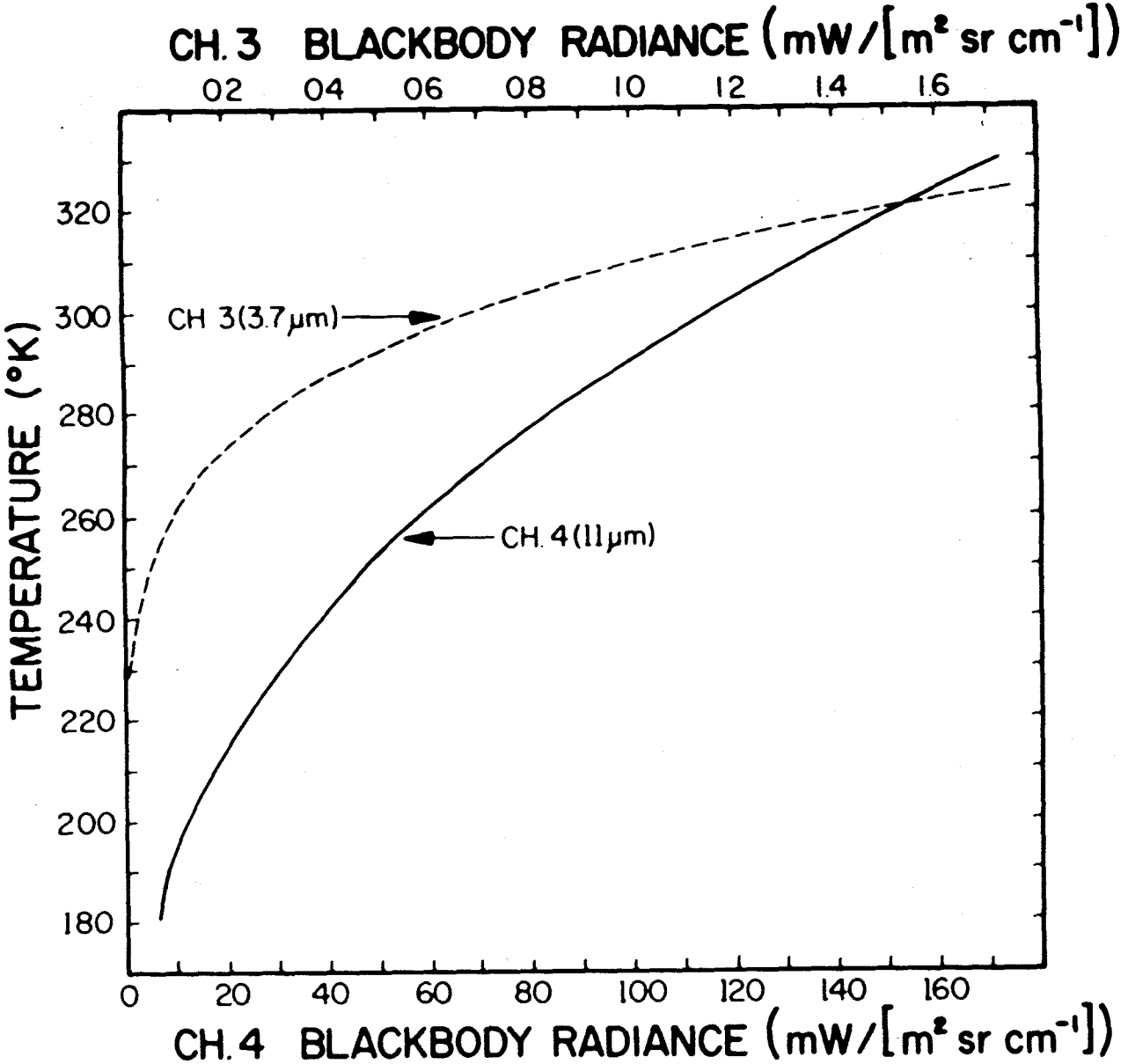

Figure 6.--Look-up table relating blackbody radiance to temperature. Solid curve (scale at bottom) for AVHRR channel 4; dashed curve (scale at top) for AVHRR channel 3.

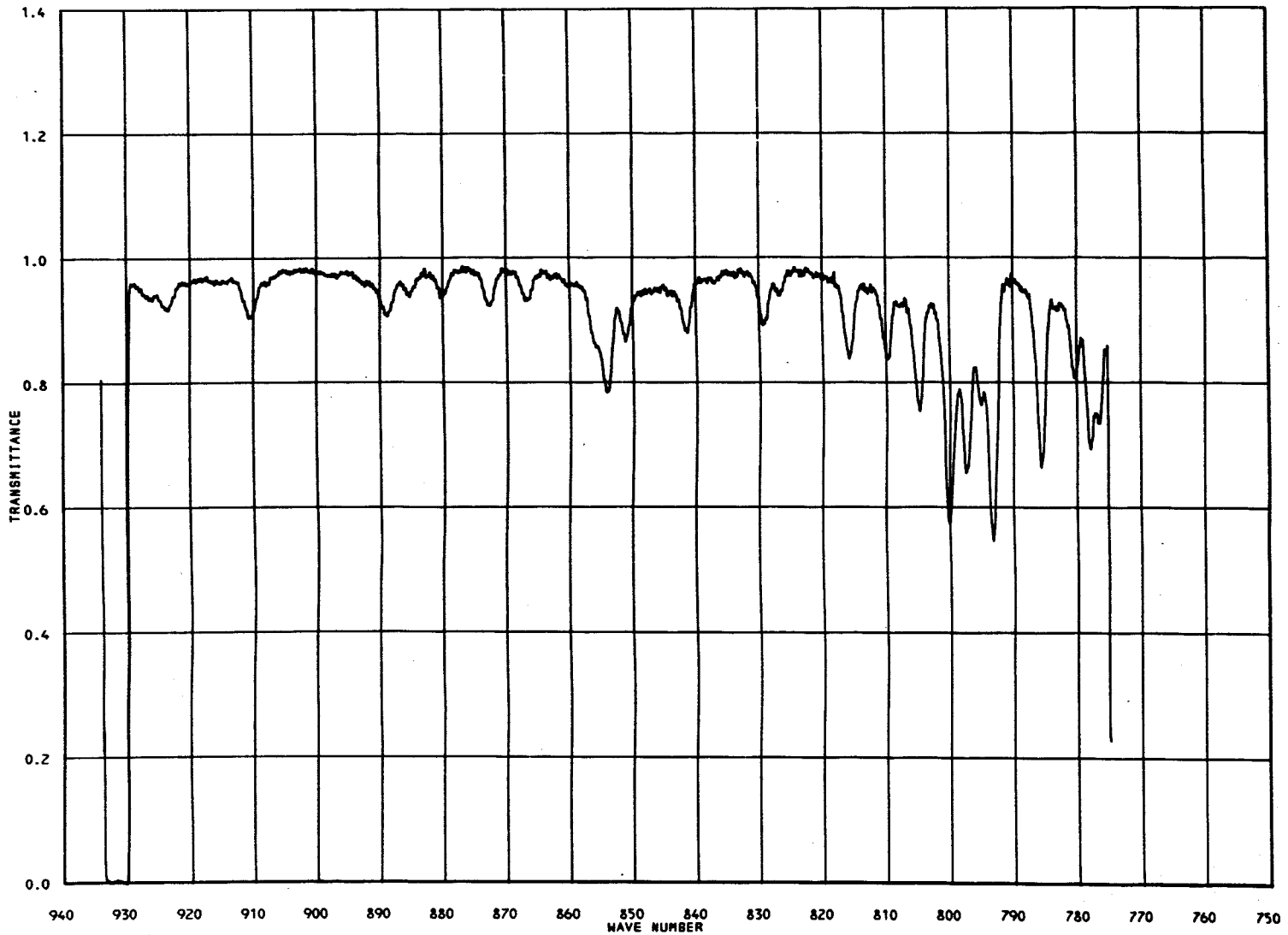

Figure 7.--Spectrum of atmospheric transmittance in 11-μm region. Spectrum taken with radiation from McMath Solar Telescope at Kitt Peak National Observatory in October 1976. Solar zenith angle was 65.5°.

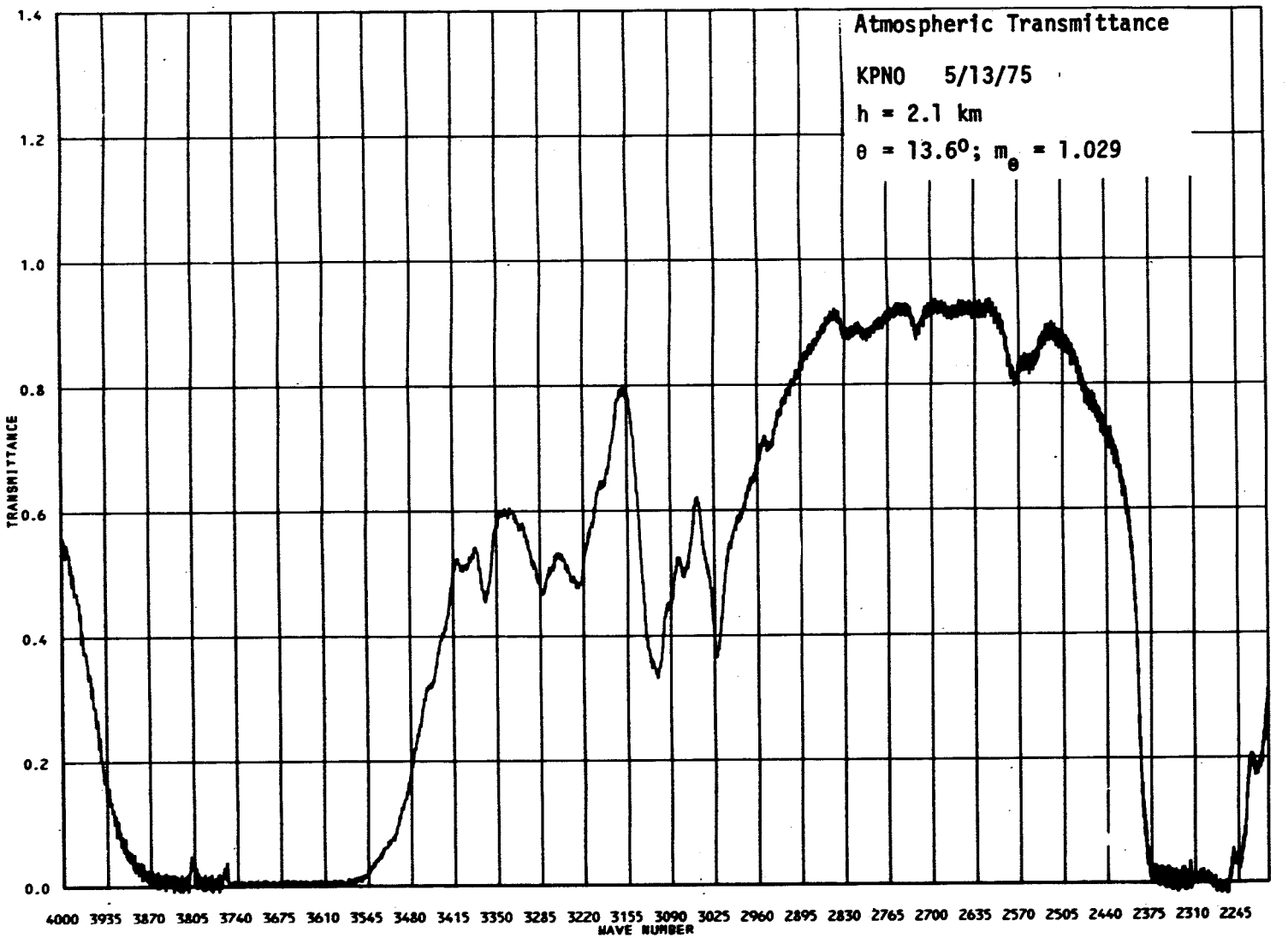

Figure 8.--As in figure 7, for 2.5- 4.5-μm region. Spectrum taken in May 1975. Solar zenith angle was 13.6°.

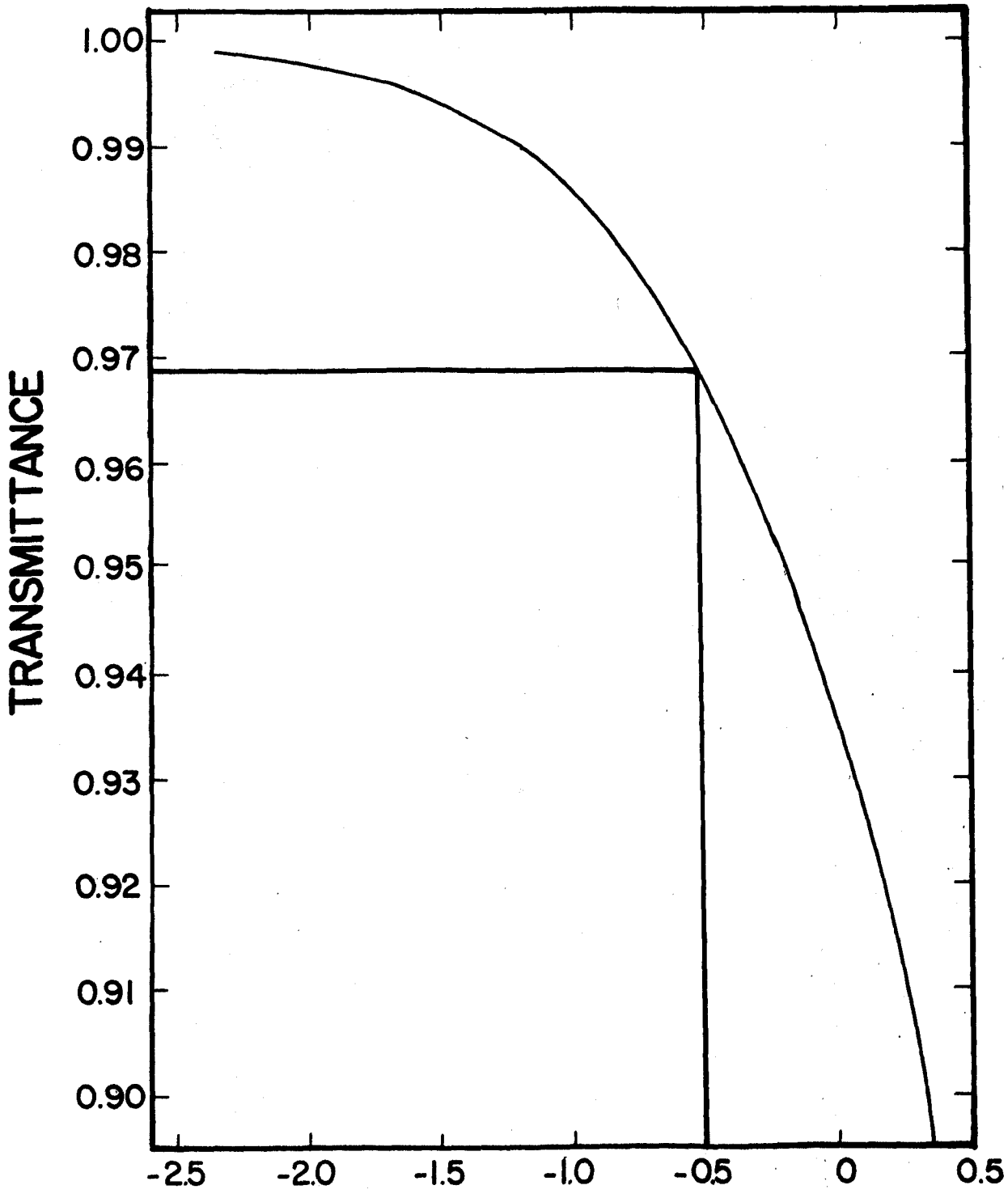

Figure 9.--Look-up table form LOWTRAN 4 (Selby et al. 1978), relating β (see text) to transmittance τ_u for uniformly - mixed gases.

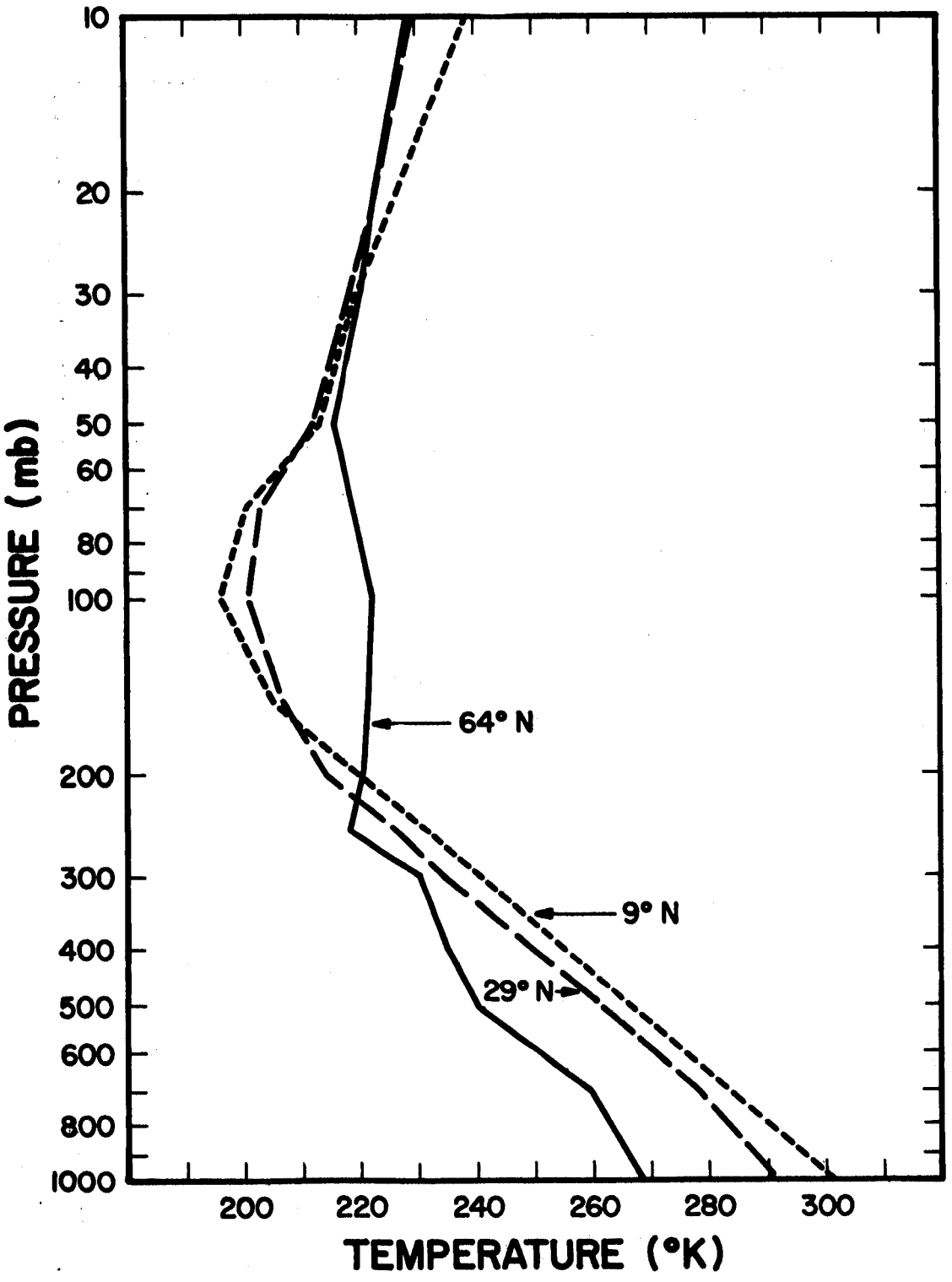

Figure 10.--Temperature profiles for three atmospheres: 64°N latitude (Ft. Greeley, Alaska, 10/14/66), 29°N latitude (Cape Canaveral, Florida, 11/18/66), and 9° latitude (Ft. Sherman, Canal Zone, 5/20/68).

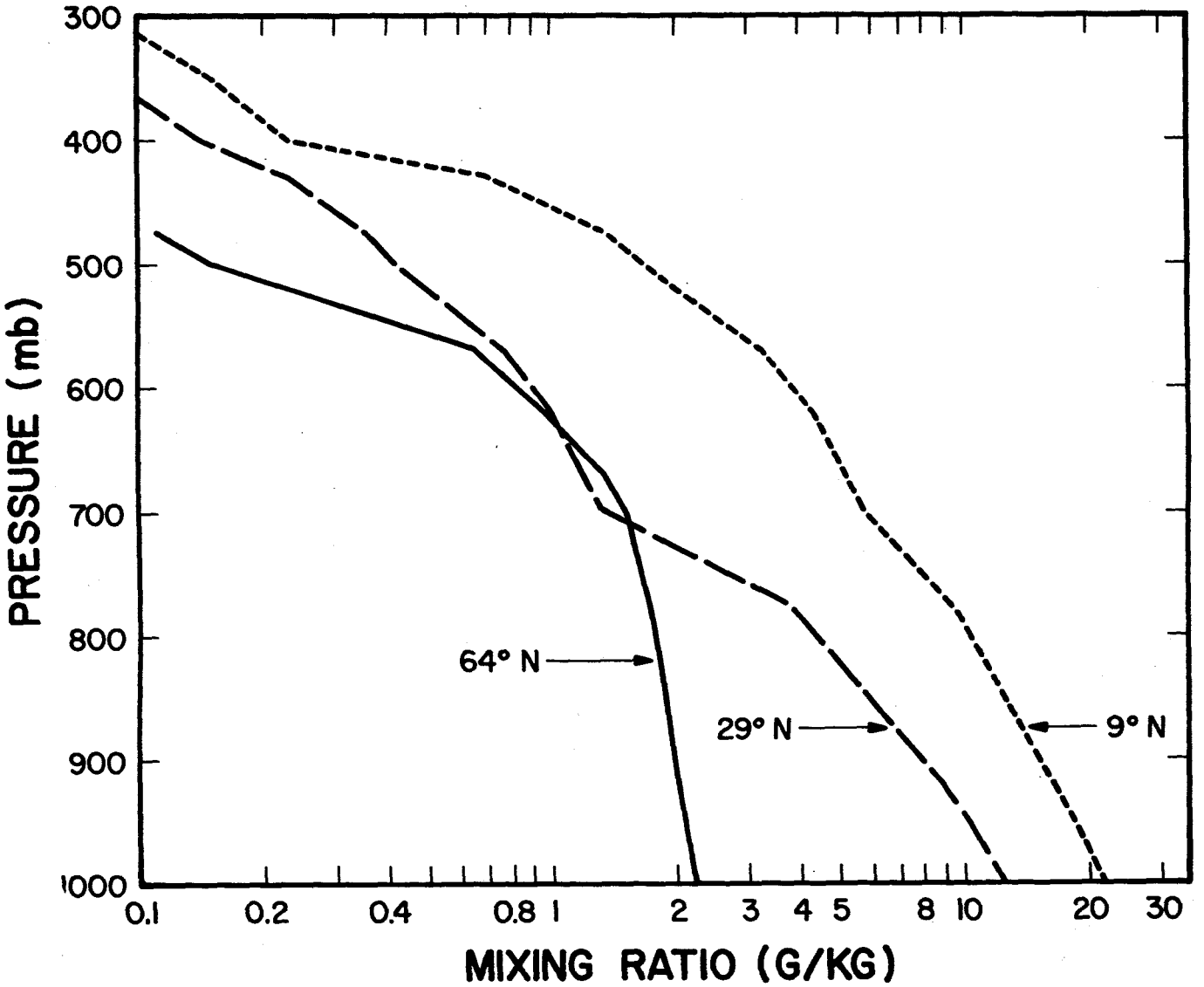

Figure 11.--Profiles of water-vapor mixing ratio for the three atmospheres of figure 10.

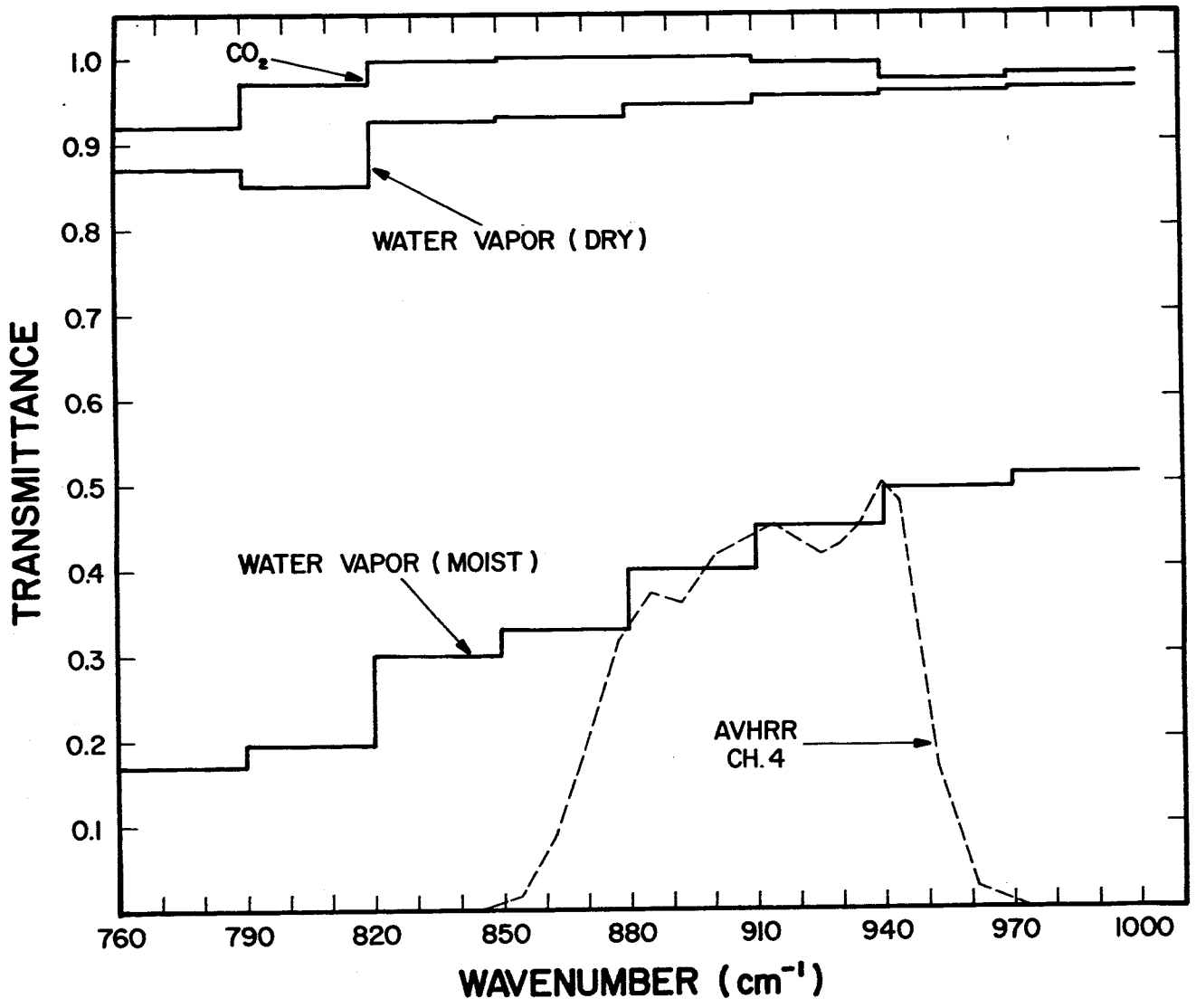

Figure 12.--Transmittances calculated for vertical path between top of atmosphere and surface in 11-μm region. Relative response in channel 4 of TIROS-N AVHRR is superimposed.

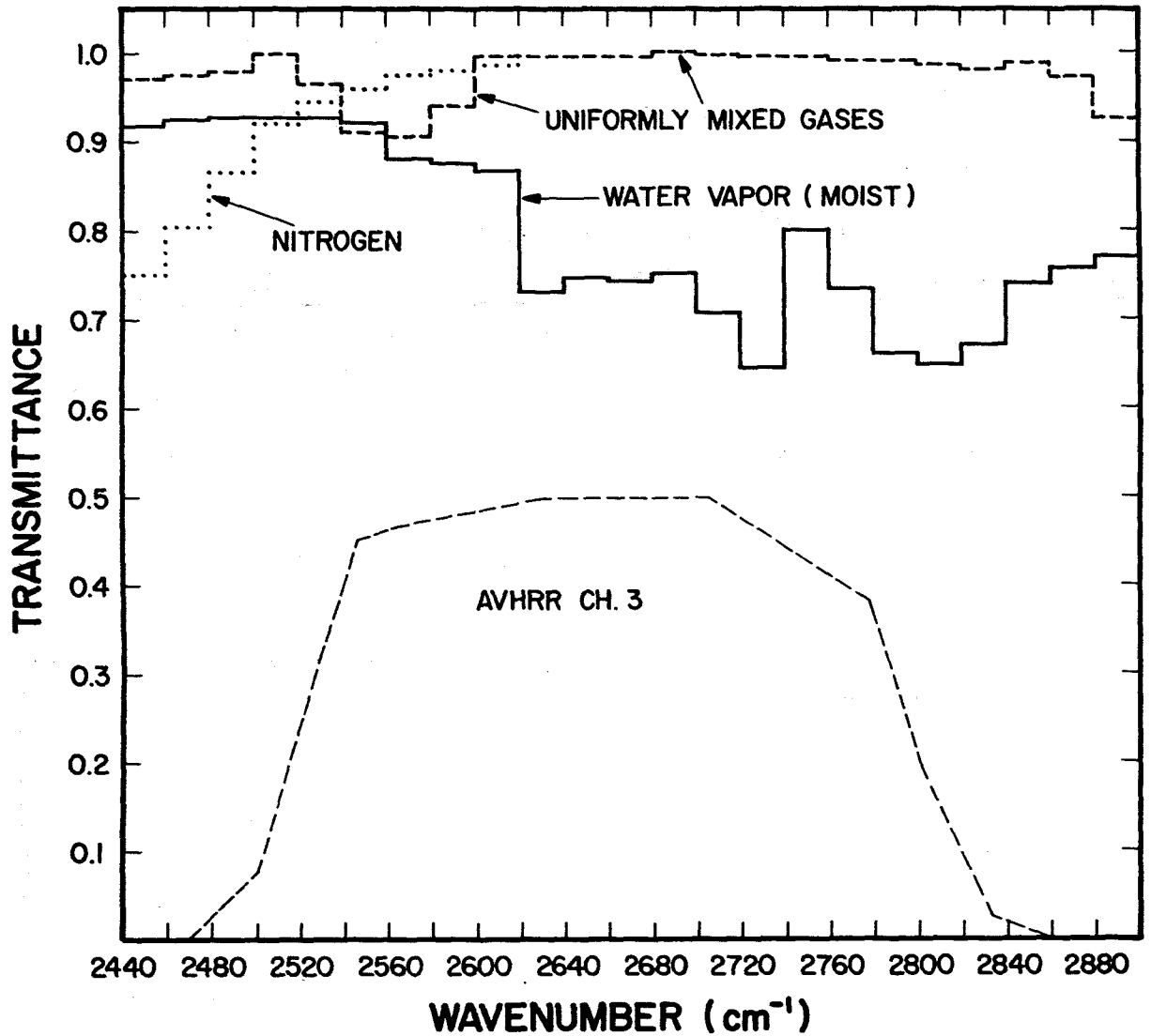

Figure 13.--As in figure 12, for 3.7-μm region and channel 3 of AVHRR.

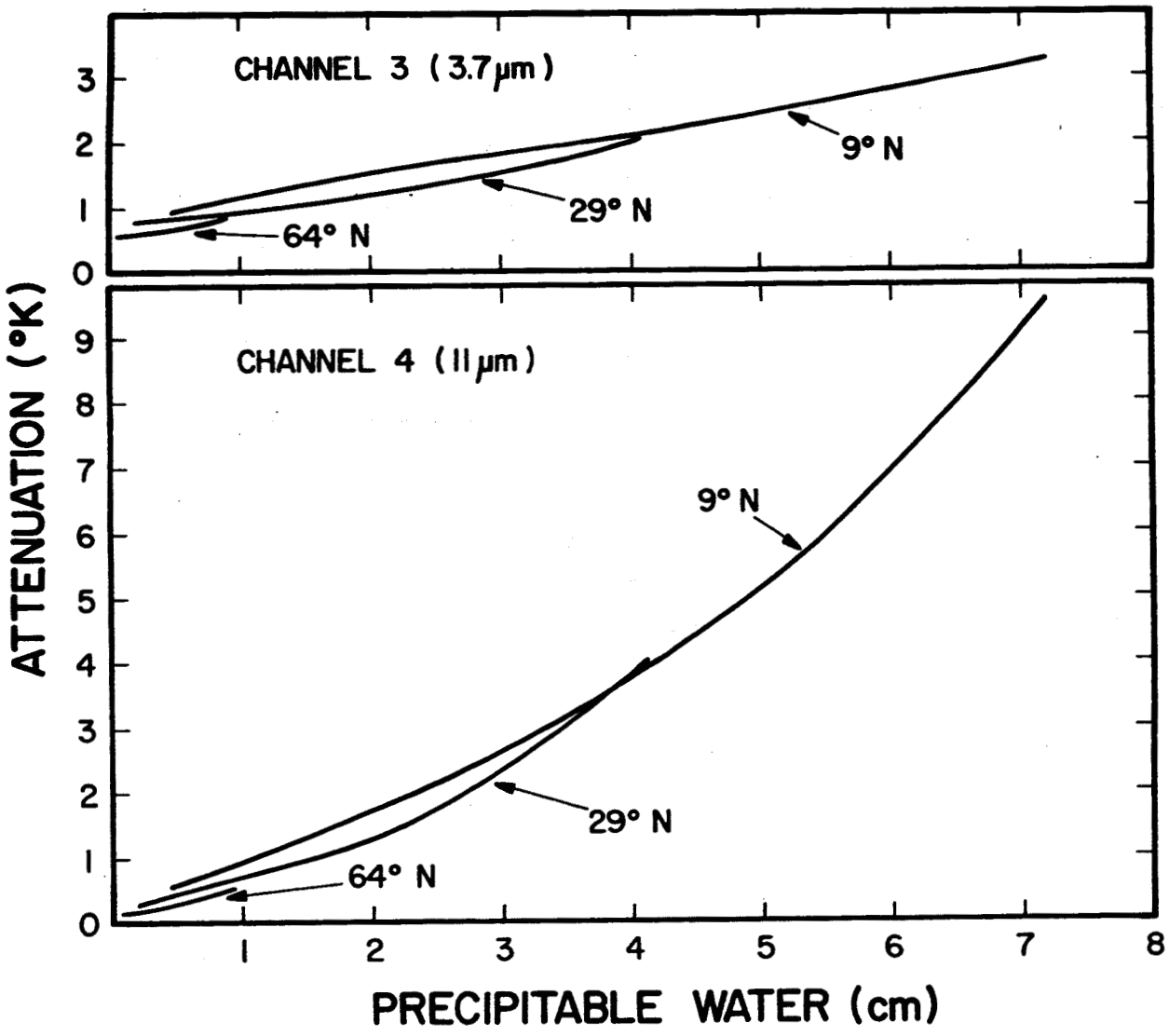

Figure 14.--Attenuation vs precipitable water for TIROS-N AVHRR.

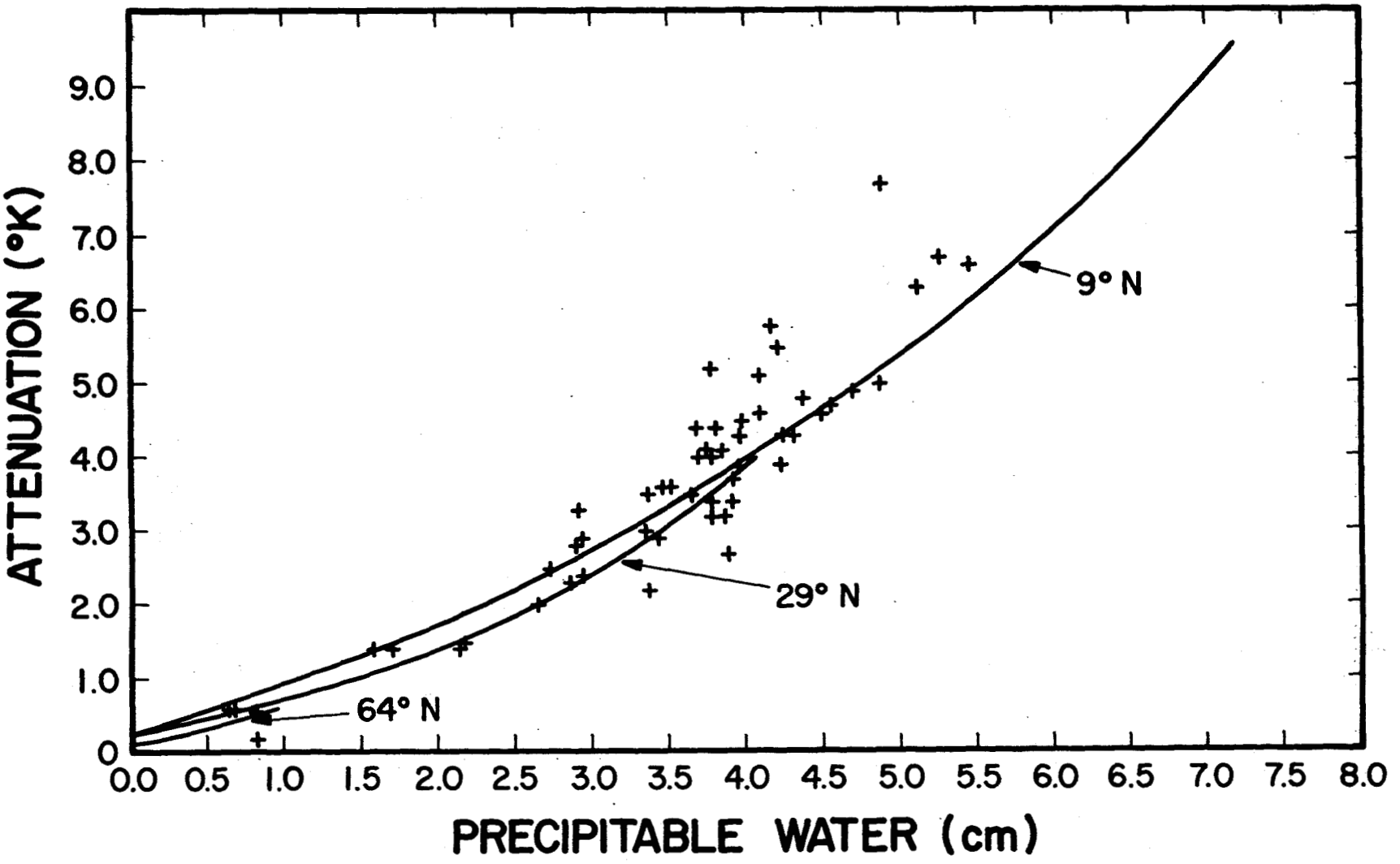

Figure 15.--Attenuation vs precipitable water for channel 4 (11 μm) of TIROS-N AVHRR. Points designated by +'s are from McClain (1979).

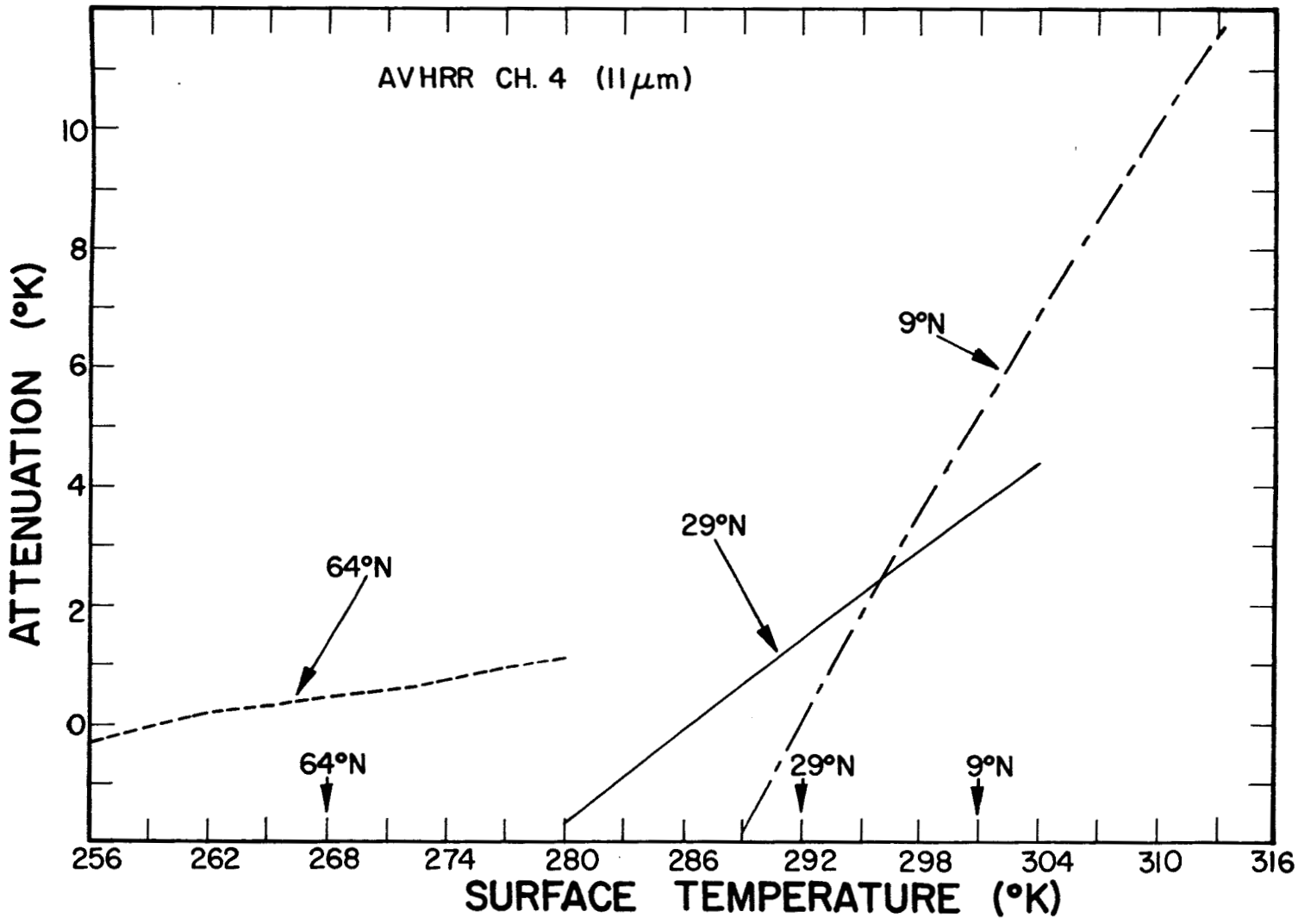

Figure 16.--Attenuation vs surface temperature for channel 4 (11 μm) of TIROS-N AVHRR, for 3 atmospheres. Arrows at bottom designate 1000 mb temperature for each atmosphere.

*U.S. GOVERNMENT PRINTING OFFICE: 1980 311-046/103 1-3

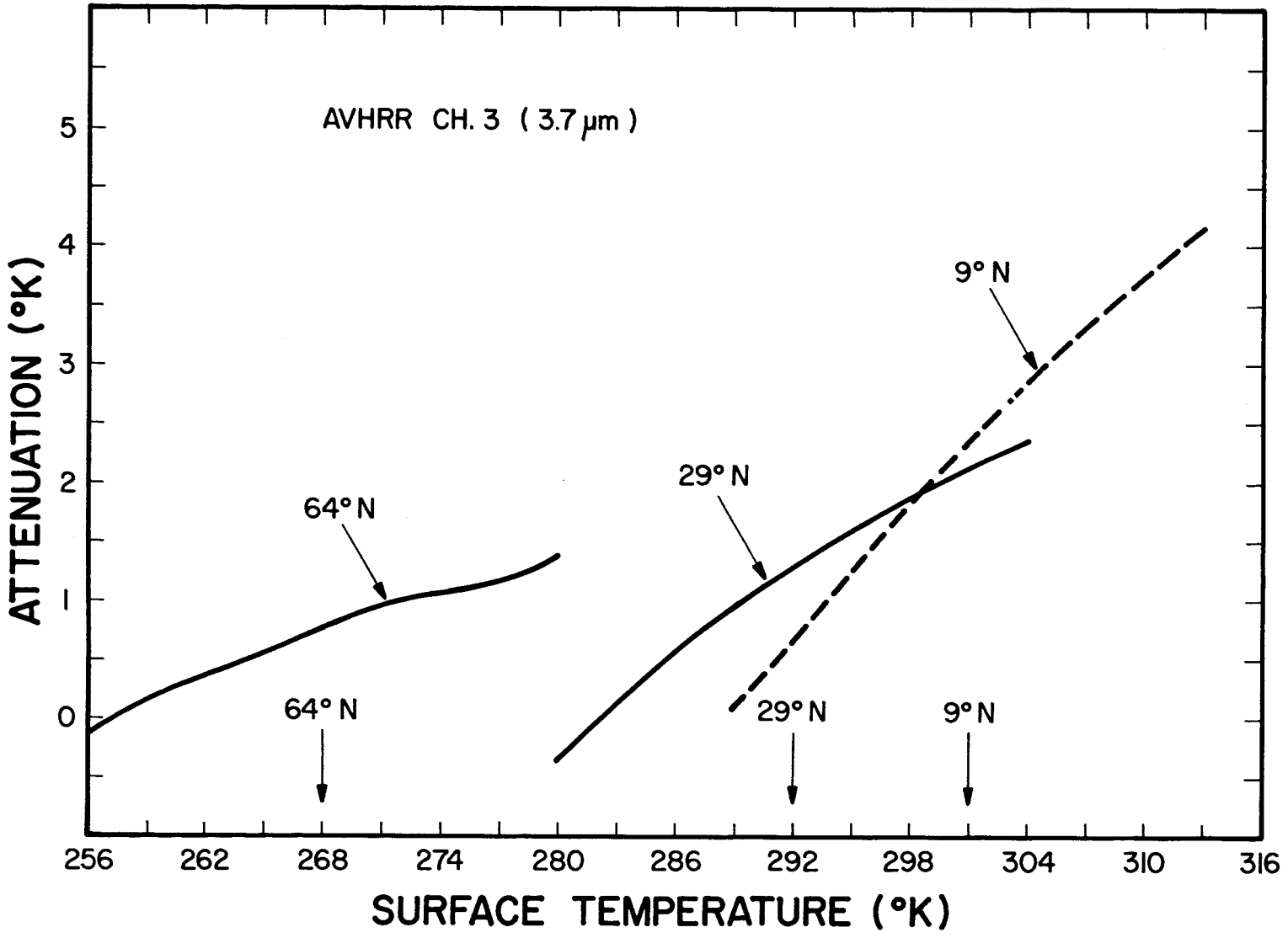

Figure 17.--As in figure 16, for channel 3 (3.7 μm) of TIROS-N AVHRR.

(Continued from inside front cover)

NOAA Technical Reports

NESS 59 Temperature Sounding From Satellites. S. Fritz, D. Q. Wark, H. E. Fleming, W. L. Smith, H. Jacobowitz, D. T. Hilleary, and J. C. Alishouse, July 1972, 49 pp. (COM-72-50963)

NESS 60 Satellite Measurements of Aerosol Backscattered Radiation From the Nimbus F Earth Radiation Budget Experiment. H. Jacobowitz, W. L. Smith, and A. J. Drummond, August 1972, 9 pp. (COM-72-51031)

NESS 61 The Measurement of Atmospheric Transmittance From Sun and Sky With an Infrared Vertical Sounder. W. L. Smith and H. B. Howell, September 1972, 16 pp. (COM-73-50020)

NESS 62 Proposed Calibration Target for the Visible Channel of a Satellite Radiometer. K. L. Coulson and H. Jacobowitz, October 1972, 27 pp. (COM-73-10143)

NESS 63 Verification of Operational SIRS B Temperature Retrievals. Harold J. Brodrick and Christopher M. Hayden, December 1972, 26 pp. (COM-73-50279)

NESS 64 Radiometric Techniques for Observing the Atmosphere From Aircraft. William L. Smith and Warren J. Jacob, January 1973, 12 pp. (COM-73-50376)

NESS 65 Satellite Infrared Soundings From NOAA Spacecraft. L. M. McMillin, D. Q. Wark, J.M. Siomkajlo, P. G. Abel, A. Werbowetzki, L. A. Lauritson, J. A. Pritchard, D. S. Crosby, H. M. Woolf, R. C. Luebbe, M. P. Weinreb, H. E. Fleming, F. E. Bittner, and C. M. Hayden, September 1973, 112 pp. (COM-73-50936/6AS)

NESS 66 Effects of Aerosols on the Determination of the Temperature of the Earth's Surface From Radiance Measurements at 11.2 m. H. Jacobowitz and K. L. Coulson, September 1973, 18 pp. (COM-74-50013)

NESS 67 Vertical Resolution of Temperature Profiles for High Resolution Infrared Radiation Sounder (HIRS). Y. M. Chen, H. M. Woolf, and W. L. Smith, January 1974, 14 pp. (COM-74-50230)

NESS 68 Dependence of Antenna Temperature on the Polarization of Emitted Radiation for a Scanning Microwave Radiometer. Norman C. Grody, January 1974, 11 pp. (COM-74-50431/AS)

NESS 69 An Evaluation of May 1971 Satellite-Derived Sea Surface Temperatures for the Southern Hemisphere. P. Krishna Rao, April 1974, 13 pp. (COM-74-50643/AS)

NESS 70 Compatibility of Low-Cloud Vectors and Rawins for Synoptic Scale Analysis. L. F. Hubert and L. F. Whitney, Jr., October 1974, 26 pp. (COM-75-50065/AS)

NESS 71 An Intercomparison of Meteorological Parameters Derived From Radiosonde and Satellite Vertical Temperature Cross Sections. W. L. Smith and H. M. Woolf, November 1974, 13 pp. (COM-75-10432)

NESS 72 An Intercomparison of Radiosonde and Satellite-Derived Cross Sections During the AMTEX. W. C. Shen, W. L. Smith, and H. M. Woolf, February 1975, 18 pp. (COM-75-10439/AS)

NESS 73 Evaluation of a Balanced 300-mb Height Analysis as a Reference Level for Satellite-Derived soundings. Albert Thomasell, Jr., December 1975, 25 pp. (PB-253-058)

NESS 74 On the Estimation of Areal Windspeed Distribution in Tropical Cyclones With the Use of Satellite Data. Andrew Timchalk, August 1976, 41 pp. (PB-261-971)

NESS 75 Guide for Designing RF Ground Receiving Stations for TIROS-N. John R. Schneider, December 1976, 126 pp. (PB-262-931)

NESS 76 Determination of the Earth-Atmosphere Radiation Budget from NOAA Satellite Data. Arnold Gruber, November 1977, 31 pp. (PB-279-633)

NESS 77 Wind Analysis by Conditional Relaxation. Albert Thomasell, Jr., January 1979.

NESS 78 Geostationary Operational Environmental Satellite/Data Collection System. July 1979, 86 pp. (PB-301-276)

NESS 79 Error Characteristics of Satellite-Derived Winds. Lester F. Hubert and Albert Thomasell, Jr. June 1979, 44 pp. (PB-300-754)

NOAA SCIENTIFIC AND TECHNICAL PUBLICATIONS

The National Oceanic and Atmospheric Administration was established as part of the Dep Commerce on October 3, 1970. The mission responsibilities of NOAA are to assess the socioeconc of natural and technological changes in the environment and to monitor and predict the state of the the oceans and their living resources, the atmosphere, and the space environment of the Earth.

The major components of NOAA regularly produce various types of scientific and technic tion in the following kinds of publications:

PROFESSIONAL PAPERS — Important definitive research results, major techniques, and special investigations.

CONTRACT AND GRANT REPORTS — Reports prepared by contractors or grantees under NOAA sponsorship.

ATLAS — Presentation of analyzed data generally in the form of maps showing distribution of rainfall, chemical and physical conditions of oceans and atmosphere, distribution of fishes and marine mammals, ionospheric conditions, etc.

TECHNICAL SERVICE PUBLICATIO ports containing data, observations, instru A partial listing includes data serials; prediction and outlook periodicals; technical manuals, training papers, planning reports, and information serials; and miscellaneous technical publications.

TECHNICAL REPORTS — Journal quality with extensive details, mathematical developments, or data listings.

TECHNICAL MEMORANDUMS — Reports of preliminary, partial, or negative research or technology results, interim instructions, and the like.

Information on availability of NOAA publications can be obtained from:

ENVIRONMENTAL SCIENCE INFORMATION CENTER (D822)
ENVIRONMENTAL DATA AND INFORMATION SERVICE
NATIONAL OCEANIC AND ATMOSPHERIC ADMINISTRATION
U.S. DEPARTMENT OF COMMERCE

6009 Executive Boulevard
Rockville, MD 20852

NOAA--S/T 80-100